

# Exploring Feasible Design Spaces for Heterogeneous Constraints

Amir M. Mirzendehtdel, Morad Behandish, and Saigopal Nelaturi

Palo Alto Research Center (PARC), 3333 Coyote Hill Road, Palo Alto, California 94304

---

## Abstract

We demonstrate an approach of exploring design spaces to simultaneously satisfy kinematics- and physics-based requirements. We present a classification of constraints and solvers to enable postponing optimization as far down the design workflow as possible. The solvers are organized into two broad classes of design space ‘pruning’ and ‘exploration’ by considering the types of constraints they can satisfy. We show that pointwise constraints define feasible design subspaces that can be represented and computed as *first-class entities* by their maximal feasible elements. The design space is pruned upfront by intersecting maximal elements, without premature optimization. To solve for other constraints, we apply topology optimization (TO), starting from the pruned feasible space. The optimization is steered by a topological sensitivity field (TSF) that measures the global changes in violation of constraints with respect to local topological punctures. The TSF for global objective functions is augmented with TSF for global constraints, and penalized/filtered to incorporate local constraints, including set constraints converted to differentiable (in)equality constraints. We demonstrate application of the proposed workflow to nontrivial examples in design and manufacturing. Among other examples, we show how to explore pruned design spaces via TO to simultaneously satisfy physics-based constraints (e.g., minimize compliance and mass) as well as kinematics-based constraints (e.g., maximize accessibility for machining).

*Keywords:* Feasible Design Space, Composing Solvers, Workflows, Maximal Elements, Sensitivity Fields

---

## 1. Introduction

Mechanical design problems require reasoning about diverse, multiple, and often conflicting objectives and constraints arising from requirements across a product’s lifecycle. The key engineering design challenge lies in traversing the trade space of these requirements to synthesize feasible designs. This challenge has recently been amplified by rapid advances in manufacturing processes. Lightweight, high-performance, and multi-material composite structures with complex geometry and material distribution can now be fabricated using various additive manufacturing (AM) processes. Yet, existing computer-aided design (CAD) systems are far behind in their representations and algorithms to navigate the high-dimensional trade spaces that grow exponentially in the number of available decisions per spatial elements. Additional functional constraints such as manufacturability, ease of assembly, motion in presence of obstacles, and aesthetics dramatically increase the trade space complexity.

Specialized domain-specific computational tools are used to generate designs that satisfy specific types of functional requirements. For example, to maximize a part’s performance with as little cost or material as possible, one may employ topology optimization (TO) tools [1–3]. In most TO approaches, an objective function is defined over a design domain in terms of the physical performance (e.g., strength and/or stiffness) with additional *constraints* on total mass or volume as well as boundary conditions (e.g., loading and/or restraints) that often account for interfaces

with other parts. TO produces valid designs with nonintuitive shapes, topologies, and material distributions that meet physical requirements, but is rarely aware of other important design criteria such as kinematic constraints. On the other hand, to ensure collision-free motion of a part in an assembly, one may need to examine its free configuration space [4–6] to guarantee collision avoidance. Similarly, for subtractive manufacturing (SM), the machinability of a designed part is predicated on whether the volume to be removed from a raw stock is accessible within the cutting tool assembly’s non-colliding configurations [7, 8]. For AM, one may need to consider the part’s morphology, minimum feature size, and skeleton [9–12]. Hybrid manufacturing (combined AM and SM) requires more complicated logical reasoning [13]. These problems require nontrivial interference analysis of shapes in relative motion that rely on different tools of reasoning than physics-driven design tools such as TO. The latter often ignore motion related constraints by considering them out-of-scope.

### 1.1. Kinematic, Physical, & Manufacturing Constraints

Generating practical designs requires *simultaneous* reasoning about shape, motion, materials, physics, manufacturing, and assembly, among other factors. For example, a machine part that moves relative to other parts in a mechanical device has to avoid collisions with both stationary and moving obstacles [14]. These requirements are imposed as *kinematic* constraints, expressed in terms of pointset containment or non-interference (Section 3.3). The same part has to sustain mechanical loads at its joints

or points of contact with other parts. These requirements are imposed as *physical* constraints, expressed in terms of (in)equalities of mathematical functions that represent physical response [15] (e.g., bounds on deflection or stress). Moreover, the part has to be manufacturable with one or more AM or SM capabilities [13]. *Manufacturability* constraints can be of both kinematic and physical types; for instance, accessibility in SM [7, 8] and post-processing of AM (e.g., support removal [16]) are of predominantly kinematic nature, whereas achieving desired material properties in AM requires in situ physical analysis [17]. With few exceptions (e.g., TO for AM with minimized support [18]) TO algorithms are not developed with manufacturability provisions built into their objective functions.

### 1.2. Generating Feasible Designs with Multiple Solvers

Different computational services, herein called *solvers*, are used to assist the design process with heterogeneous constraints by providing either *analysis* tools to evaluate the performance of one or more given designs, or *synthesis* tools to generate one or more designs that satisfy a given set of performance criteria analysis. We distinguish between these two types of solvers as *forward* and *inverse* problem solvers (‘FP/IP-solvers’), respectively (Section 3). Specifically, *generative design* tools are IP-solvers which solve the inverse problem by systematically generating candidate designs and evaluating their performance (using FP-solvers) to guide refinement of designs until the criteria are met.

It is unlikely that a single IP-solver is capable of simultaneous reasoning about all design criteria (e.g., objective functions and constraints). Therefore, a typical computational design workflow requires carefully organizing and reasoning about several multidisciplinary solvers to address heterogeneous design criteria. While every IP-solver reasoning about a *subset* of these criteria may produce designs that are feasible (and ideally, optimal) only with respect to the specific criteria it considers, it provides no guarantees about the rest of the criteria. Different IP-solvers are thus likely to generate designs distinct from one another, while none of them simultaneously satisfies all criteria. Except for extremely simple criteria, it appears impossible to combine these solutions in any obvious way that preserves the constraints satisfied separately by each solver, or at least provides the best compromise. Even if such a solution exists, there may not exist any particular ordering of these solvers to find it, simply because each solver performs *premature optimization* with regard to the subset of criteria it cares about.

Consider the problem of designing a car hood latch (adopted from [14]). An initial design domain with boundary conditions is provided, and the goal is to find a design that is as stiff as possible with the least mass. Moreover, the latch has to be free to rotate clockwise by 20 degrees around a revolute joint, without exiting the initial design domain, so that it would not collide with other parts

that are possibly outside that envelope. Functional load-bearing surfaces where the latch mates with other parts are shown in Fig. 1. All feasible designs must retain these surfaces as specified. The said requirements immediately suggest using two IP-solvers that are well-positioned to deal with them (each solver satisfying a subset of them):

- Let **Un sweep** [19] be a solver that generates a design that remains within a given region of space while moving according to a prescribed motion (in this case, a clockwise rotation of 21 degrees).
- Let **PareTO** [20] be a solver that, starting from an initial design, generates a design on the Pareto front of the two objectives (compliance and mass), i.e., one that satisfies the stiffness requirement and the given boundary conditions with minimal mass.

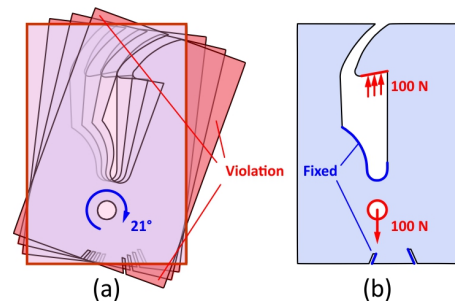


Figure 1: Functional requirements for designing a car hood latch, including (a) containment under given motion after assembly; and (b) boundary conditions on interfaces for assembly.

Using these solvers separately, one may generate two distinct designs, as illustrated in Fig. 2. However, there is no clear operation with which to combine these two, in order to generate a design that satisfies both kinematics and physics-based constraints. For example, the intersection of the two designs, shown in Fig. 2 generates a design that does not violate the constraints satisfied by **Un sweep**, because every subset of the unswept volume also satisfies the containment constraints. However, the constraints satisfied by **PareTO** are no longer satisfied, because the load paths are changed due to the changed topology and the compliance target is no longer met.

In this case, **Un sweep** has a property that its solution can be interpreted not as a single design, but as a representation of all designs that satisfy the containment constraints. This family of designs is *closed under set intersection*, i.e., intersecting any of the feasible designs with another set leads to another feasible design. Similarly, **PareTO** can generate a family of designs that satisfy compliance requirements for different mass budgets. However, this family is not closed under set intersection. The goal of this paper is to show how we can exploit such information to organize the design workflows such that they produce solutions that satisfy all criteria.

It is possible to obtain a feasible solution to the latch design problem by using the same set of IP-solvers, if the

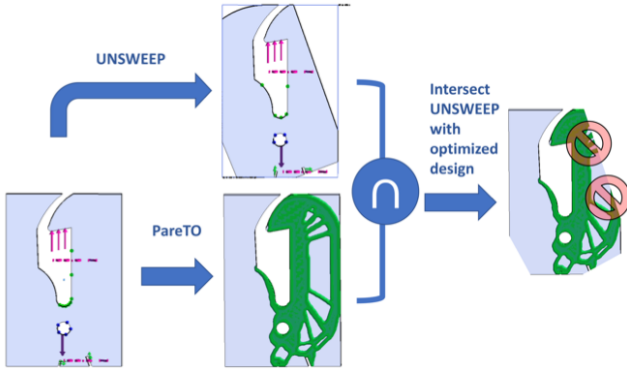


Figure 2: Two partially feasible designs are generated separately by two solvers. Each solver optimizes for a subset of constraints. Arbitrarily combining them (e.g., via set intersection in this example) may result in an infeasible design with respect to all constraints.

workflow is organized differently, as shown in Fig. 3. Suppose we first solve for the containment constraint using UnswEEP and generate a valid design that does not exit a given envelope while moving. We can use this design as the initial design input to PareTO and optimize its shape and topology to achieve the compliance target with minimal mass. This approach works because PareTO is a material reducing solver, i.e., its solutions remain strictly contained within the initial design. Hence any design generated downstream will be faithful to the containment constraint that was satisfied upstream. The same argument is not true if the order of applying the solvers is swapped. There is no reason to believe that applying UnswEEP to a topologically optimized solution of PareTO will remain on the Pareto front. The fundamental differences between the two IP-solvers should be taken into account when deciding on their arrangement in a workflow—in this case, choosing between parallel or sequential execution and the proper order for the latter. We elaborate on these differences in the classification of solvers in Section 3.

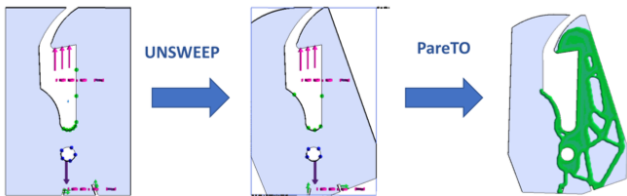


Figure 3: Both constraints can be satisfied by first finding a shape that satisfies the containment constraint and then using this shape as the input to TO (or any other material reducing IP-solver).

Figure 4 shows a one-parametric family of solutions on the Pareto front obtained when using mass and compliance as competing objectives. PareTO provides a clear advantage over classical TO with a single solution, by producing many alternatives *some* of which might satisfy additional constraints that were not accounted for in TO. This *generate-and-test* approach is plausible, and in fact, is a common strategy for dealing with heterogeneous con-

straints. However, it turns out that none of the Pareto-optimized designs in this case will not remain within the envelope after a clockwise rotation of 21 degrees.

In general, a good rule of thumb to organize solvers in a workflow is to call the ones that produce the broadest families of designs earlier. The upstream IP-solvers should generate a large number of designs, as opposed to fixing one or few designs, to provide more flexibility for downstream solvers. The downstream solvers can be FP-solvers, testing for new constraints, or IP-solvers, applying further optimization. However, each solver may prematurely optimize designs that may fail evaluation criteria considered in downstream solvers. The “blind” process of generating and testing designs without carefully considering properties of the workflow – and the associated feasible design space for each solver in the workflow – will scale poorly with increasing number of constraints/solvers and their complexity. A systematic approach to arranging solvers into workflows that guarantees satisfying new constraints without violating the already satisfied constraints is much demanded, and is the subject of this paper.

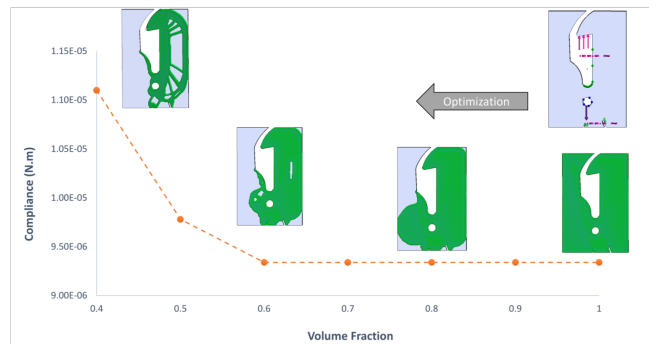


Figure 4: None of the topologically optimized design alternatives obtained from applying PareTO to the initial design will satisfy the containment constraint. Generate-and-test does not always work.

### 1.3. Contributions & Outline

The main contributions of this paper are:

1. classification of IP-solvers based on the properties of design constraints (e.g., locality and continuity) that each solver can handle;
2. organization of computational design workflows with heterogeneous constraints into two stages of design space ‘pruning’ and ‘exploration’, where pruning provides the feasible design space for exploration;
3. reconciling set constraints with inequality constraints and deriving conditions under which they can be expressed in a strictly local (i.e., ‘pointwise’) fashion;
4. pruning *design spaces*, treated as *first-class entities*,<sup>1</sup>

<sup>1</sup>In the lexicon of programming languages, a construct is said to have first-class status if it can be passed as an argument, returned from a subroutine, or assigned into a variable [21].

by intersecting their representative maximal elements defined implicitly by pointwise constraints;

5. strategies to compose FP-solvers into a generative and iterative design process by combining kinematic, manufacturing, and physical constraints; and
6. illustrating real-world design problems solved using multidisciplinary solvers, which are rarely addressed in the (otherwise siloed) areas of related research.

In Section 2, we review some of the recent works in related areas of computational design and manufacturing.

In Section 3, we present basic definitions (FP/IP-solvers, global vs. local constraints, and design/performance space terminology). We present a classification of solvers based on the types of constraints they can handle, and propose a systematic approach for organizing them into workflows.

In Section 4, we show that an important class of constraints can be satisfied upfront by pruning the design space in the early stages without premature optimization, allowing flexibility for downstream design decisions. The feasible design subspaces are described uniquely and completely by their *maximal elements*. These representative elements are, in turn, implicitly defined by a point membership classification (PMC) test implemented in terms of strictly local (i.e., ‘pointwise’) constraints. We demonstrate examples of kinematics-based constraints that appear in assembly, packaging, and manufacturing.

In Section 5 we deal with more general global and local constraints, including (in)equality constraints that specify physics-driven requirements or manufacturability.

We use a Pareto-tracing levelset topology optimization (PareTO) [20] which uses fixed-point iteration to satisfy multiple design criteria guided by augmented TSFs. We demonstrate that accessibility constraints can be incorporated in TO by filtering the augmented TSF using the overlap measure of cutting tool and optimized part.

We conclude in Section 6 by a discussion of the limitations of our approach and proposed future directions.

## 2. Related Work

Real-world design problems often involve solving multi-objective optimization problems where the goal is to find the best trade-off between multiple competing objective functions. Classical methods such as linear programming (e.g., the ‘simplex’ algorithm), nonlinear programming (e.g., the steepest descent and conjugate gradients), or Newton-Raphson [22] are limited to single-objective optimization problems. Even for single-objective optimization, finding the global optimum is NP-hard [23]. Numerous approaches have been developed to converge to locally optimal solutions in reasonable computation time to multi-objective problems across different disciplines.

Unlike single-objective optimization, a total ordering for feasible solutions may not be possible in multi-objective optimization, i.e., there may not exist a single “best”

solution due to competing objectives. However, feasible solutions may be partially ordered according to *Pareto efficiency*—also known as Pareto–Koopmans efficiency or dominance [24, 25]. Pareto-optimal solutions are locally optimal (according to Pareto-efficiency) where improving one objective comes at the expense of at least one other objective [26]. The collection of all Pareto-optimal solutions is referred to as a *Pareto front*, which represents a curve, surface, or higher-dimensional manifold in the design space for two, three, or higher number of competing objectives, respectively. Tracing a Pareto front is a key challenge in multi-objective and multi-disciplinary design optimization. We will not attempt an exhaustive review of all approaches such as gradient-free methods including rule-based techniques [27–30] and evolutionary algorithms [31–35]. Rather, we focus on a special class of algorithms that automatically generate designs on the Pareto front of multiple objectives given an initial design.

TO [3, 36, 37] has emerged as a practical class of computational methods for designing high-performance lightweight structures and has been applied in numerous areas such as designing automobiles components [38], aircraft components [39, 40], spacecraft modules [41], cast parts [42], compliant mechanisms [43], and many other products. Numerous approaches such as density-based [44–46], levelset-based [47, 48], and evolutionary [49–51] methods for TO have been developed.

### 2.1. Optimal Design for Manufacturing

TO typically focuses on optimizing designs for performance (e.g., physical response to loads during operation) but less on other important factors such as *manufacturability*. Apart from traditional processes such as machining and molding, more recent technologies such as AM have introduced the ability to fabricate complex topologically optimized designs while presenting new manufacturing challenges [52]. Process limitations must be considered *during* the design/optimization stage as much as possible to avoid repeated prototyping and iterations until the optimized designs are manufacturable. Specifically, applying corrections to the geometry [9] or topology [11] of a solution *after* TO to make it manufacturable may sacrifice the achieved optimality.

One solution is to impose *design rules* obtained from domain expertise and experience. These rules relate specific combinations of shape, materials, and process to impose simplified constraints that can be built into the TO framework to restrict the feasible design space. For example, when designing for AM via fused deposition modeling using polymers, one should require that all facets oriented at an angle greater than 45 degrees with respect to the build direction be supported with additional scaffolding material. When designing for casting and injection molding processes, one should ensure that the part has features of almost uniform thickness and no entrapped holes are present, so that the mold can be removed and the molten material cools down uniformly throughout the part

[53, 54]. When designing for wire- or laser-cutting, one should ensure that the final design has a uniform cross-section, i.e., is 2.5D along the cutting direction. These constraints can be imposed during TO through filtering of the sensitivity field as illustrated in Fig. 5.

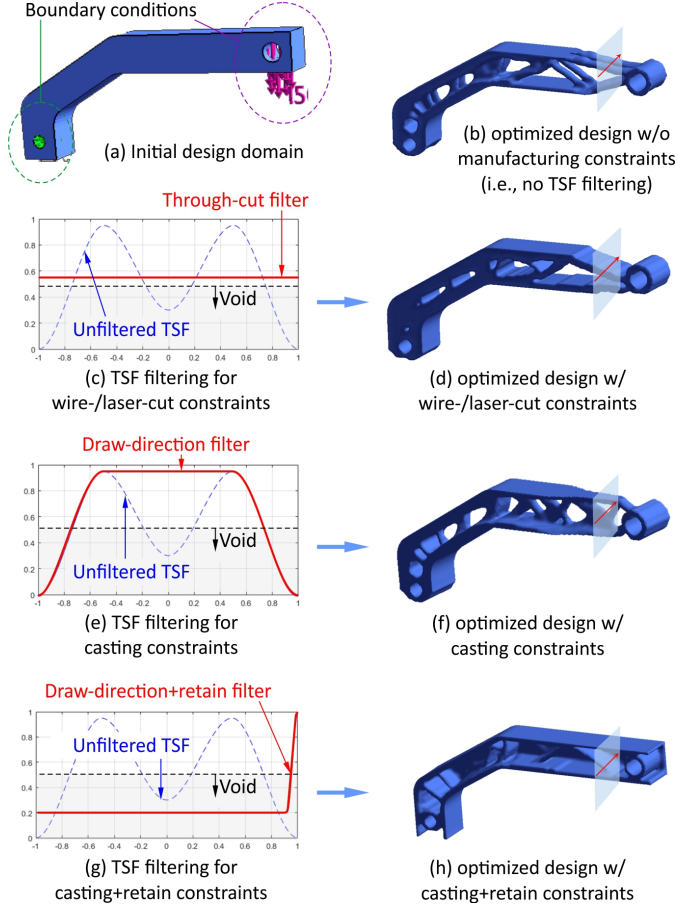


Figure 5: Examples of enforcing manufacturability constraints by TSF filtering. Different filters (c, e, g) – plotted along the cross-sections shown on the right – produce different solutions (d, f, h).

Another important AM consideration is the manufacturing resolution, which can be directly incorporated into the TO algorithm as a minimum feature size constraint through either local gradient constraints [55] or TSF filtering [43] (Fig. 6). It is also possible to reduce the amount of support structure needed in an AM by either finding a good build orientation or TSF filtering. Build orientation optimization often involves solving a multi-objective problem taking into account other factors such as surface quality [56, 57], build time [56], or manufacturing error [58]. TSF filtering, on the other hand, can be achieved by penalizing overhang surfaces [59, 60], penalizing undercut surfaces [61], or augmenting new TSFs [18].

Other AM constraints may not be as straightforward. For instance, optimizing designs with respect to shrinkage and warpage during material phase changes within the AM process may require solving a multi-physics problem at every iteration [17, 63]. Characterizing material

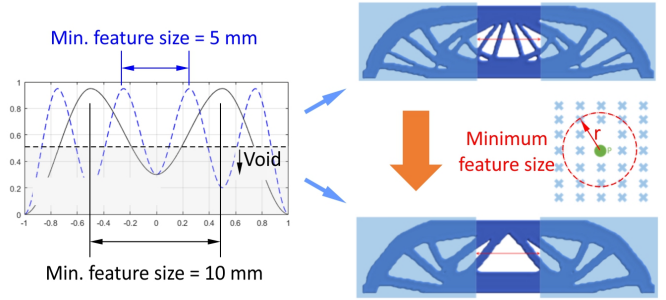


Figure 6: Constraining minimum feature size via TSF filtering [62].

properties of AM parts is also challenging due to process-induced anisotropy. Lack of inter-layer adhesion and varying thermal history at every point can introduce unintended porosities and consequently affect material behavior. Although there are initial results for considering anisotropy in TO under certain assumptions [64], solving the problem by simultaneously optimizing the geometry, topology, and process parameters involves costly in-situ manufacturing simulation or process planning [7, 13].

## 2.2. Design for Motion-Related Constraints

In addition to the above examples of performance and manufacturing requirements, there are other important design criteria that involve spatial reasoning about the interactions of moving (translating and rotating) shapes such as collision avoidance, packaging, robot motion planning, and accessibility analysis. These requirements cannot be easily enforced by design rules, TSF filtering, or other techniques commonly used in TO. Rather, they are often expressed as *set constraints*, i.e., statements in the language of sets (e.g., in terms of affine transformations, Boolean operations, and containment) rather than the language of real-valued functions used for (in)equality constraints in TO. A broad class of inverse problems in practical design and manufacturing reduce to solving set constraints formulated in the configuration space of rigid motions [6, 65–67].

Although the problems with set constraints are common and of significant importance, they are not mainstream in design/optimization workflows due to non-smoothness and computational intensity [68]. There are instances of TO frameworks that deal with motion-related problems in an ad hoc manner; for instance, in modeling collision and contact when designing compliant mechanisms [69] or parts made of hyperelastic materials that undergo large deformations part [70, 71]. However, it is not immediately obvious how set constraints can be incorporated in a *systematic* fashion into the design/optimization process without incurring prohibitive computation costs of spatial analysis at every iteration. The next section presents a different classification of constraints that enables design space pruning and exploration, in which set constraints are also restated in terms of (in)equalities of functions.

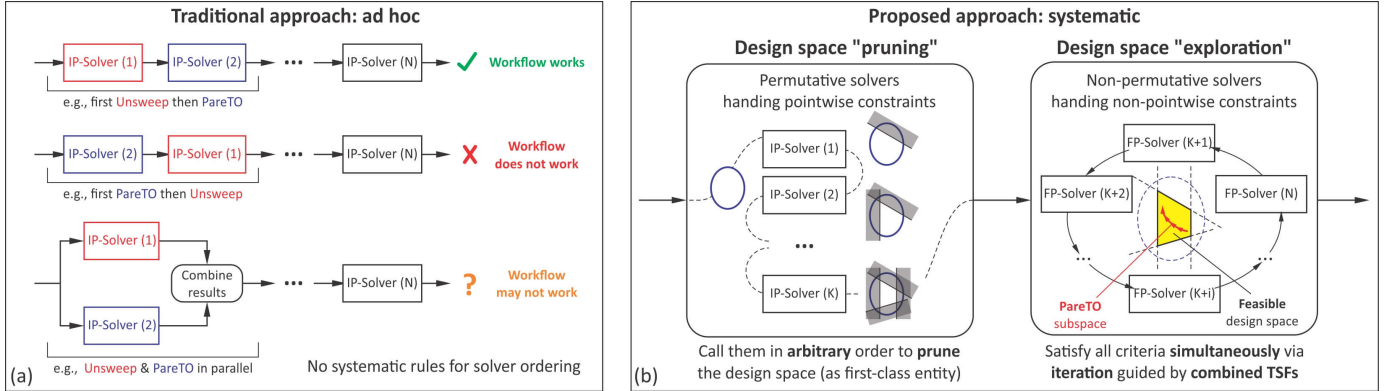


Figure 7: Solving heterogeneous (e.g., kinematic, physical, and manufacturing) constraints with multidisciplinary solvers is difficult. Each solver might make decisions with care for its target subset of constraints while potentially violating the rest of the constraints. (a) Arranging multiple solvers sequentially may work in some orders and fail in others, depending on what properties they preserve. Parallel composition requires combining solutions in ways that do not always preserve the properties either. (b) We propose a systematic two-phase approach (Section 3.4) to design space pruning (Section 4) and design space exploration (Section 5). The former invokes IP-solvers in an arbitrary order to cut out the infeasible design subspace without premature optimization. The latter navigates the pruned design space by fixed-point iterations over FP-solvers. Section 3 addresses the question of how to divide a given collection of solvers into these two groups.

### 3. Classifying Solvers and Constraints

In this paper we restrict our attention on solvers that reduce material from a bounded domain in 2D and 3D space to generate designs. Our focus will be on the properties of *constraints* embedded within computational solvers to reason about their ordering in the workflows.

When all objectives and constraints cannot be handled by a single solver, current practice relies on a case-by-case domain-specific analysis to properly construct workflows. Figure 7 (a) depicts examples of combining Unsweep and PareTO illustrated in Section 1.2. An arrangement that works in one case may not work in another.

In contrast, we present a systematic approach for organizing solvers into workflows by first classifying solvers into two fundamentally different types:

1. *Design space pruning* solvers restrict the feasible design space by pruning the subspaces that violate one or more design criteria. They are permutative, meaning that they can be called at the beginning of the design workflow in an *arbitrary order*. By directly operating on the design subspaces as first-class entities, they postpone optimization to downstream solvers.
2. *Design space exploration* solvers *simultaneously* explore the (pruned) design subspaces for optimized solutions. In this paper, we choose a well-studied Pareto front tracing approach (PareTO) [72] to efficiently navigate the trade space of multiple objectives.

Figure 7 (b) illustrates the framework. In this section we present some terminology and a classification of design criteria based on which the solvers can be grouped into the above two classes. We formalize this two-phase approach in Section 3.4 and discuss how to implement each phase in depth with examples in Sections 4 and 5, respectively.

#### 3.1. Design & Performance Spaces

Throughout this paper, a ‘design’  $\Omega$  refers to a computational model of a *single* designed artifact. We begin the process by specifying a bounded *design domain*  $\Omega_0 \subset \mathbb{R}^d$  ( $d = 2$  or  $3$ ) whose corresponding *design space*  $\mathcal{D}$  is the collection of all ‘solids’, i.e., closed-regular semianalytic pointsets in  $d$ -space,<sup>2</sup> contained within the design domain. We use the notation  $\mathcal{D} = \mathcal{P}^*(\Omega_0)$  (read: “solid powerset” of  $\Omega_0$ ). This definition is sufficient for geometric modeling of parts with homogeneous and isotropic material properties. We initially restrict our attention to this subclass of artifacts, as considered in classical solid modeling [73]. Our goal is to first illustrate nontrivial challenges in designing with multiple solvers before introducing the additional complexity of multiple materials, heterogeneity, or anisotropy. However, the concepts introduced hereafter can (in principle) be generalized beyond solids.

The ‘performance’ of a given design  $\Omega \in \mathcal{D}$  is an  $n$ -tuple  $\mathcal{A}(\Omega) := (\mathcal{A}_1(\Omega), \dots, \mathcal{A}_n(\Omega))$ . Think of the *performance space* as a product space  $\mathcal{P} := (\mathcal{F}_1 \times \dots \times \mathcal{F}_n)$ , where each  $\mathcal{F}_i$  is a class of fields, i.e., each  $\mathcal{A}_i \in \mathcal{F}_1$  is an integrable field  $\mathcal{A}_i(\Omega) : \Omega_0 \rightarrow \mathbb{Q}_i$  over the design domain  $\Omega_0$  whose value at a given “query point”  $\mathbf{x} \in \Omega_0$  is denoted by  $\mathcal{A}_i(\mathbf{x}; \Omega) := (\mathcal{A}_i(\Omega))(\mathbf{x}) \in \mathbb{Q}_i$ . Examples of such fields are:

- binary-valued fields ( $\mathbb{Q}_i := \{0, 1\}$ ), used to describe indicator functions of regions of interest within the design domain such as non-manufacturable features [7, 8] or regions requiring design correction [9].
- integer-valued scalar fields ( $\mathbb{Q}_i := \mathbb{Z}$ ), used to characterize local topological properties of 3D printed parts [11, 12] or to classify atomic units of manufacturing in hybrid (combined AM and SM) manufacturing [13].

<sup>2</sup>A closed-regular set is defined as a set that equals the closure of its interior (i.e., is homogeneously 3D) [73].

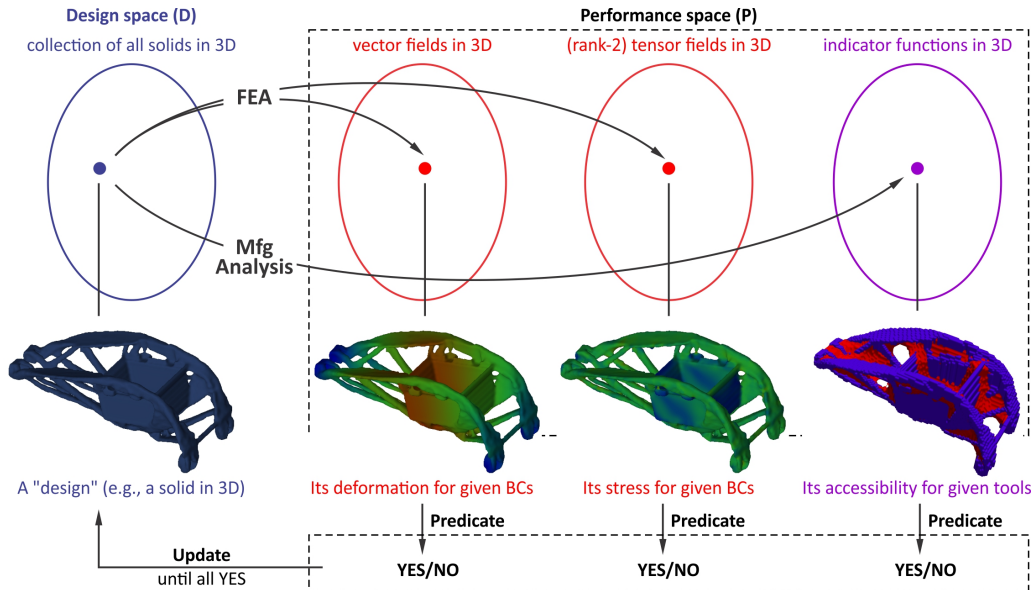


Figure 8: (a) FP-solvers (e.g., FEA and manufacturability analysis) map an instance of the design space (i.e., a “design”) to an instance of the performance space (i.e., a “field-tuple”). Predicates are defined to decide whether the design is satisfactory with respect to *constraints* in terms of performance variables. An IP-solver modifies the design until all constraints are satisfied.

- real-valued scalar fields ( $\mathbb{Q}_i := \mathbb{R}$ ), 3D vector fields ( $\mathbb{Q}_i := \mathbb{R}^3$ ), and higher-rank tensor fields used to represent distributed physical quantities such as displacement, velocity, stress, strain, and so on [15], or manufacturability measures [10].

### 3.1.1. Forward Problem in Physics & Kinematics

Forward problem solvers (FP-solvers) map a given design instance to one or more performance fields, hence can be viewed as implementations of one or more maps  $\mathcal{A}_i : \mathcal{D} \rightarrow \mathcal{P}_i$ . The entire forward problem, solved by one or more FP-solvers, can be viewed as a single map from design space to performance space  $\mathcal{A} : \mathcal{D} \rightarrow \mathcal{P}$ , which has a unique outcome for a given design.

For example, consider a finite elements analysis (FEA) FP-solver that computes (discretized forms of) a displacement field  $\mathbf{u}_\Omega := \mathcal{A}_1(\Omega)$  for small deformations [15] of a given design  $\Omega \in \mathcal{D}$  due to boundary conditions such as restraints and external forces (Fig. 8). It is also important to compute the stress field  $\sigma_\Omega := \mathcal{A}_2(\Omega)$ , which depends locally on displacement and material properties (e.g., the linear elasticity law). The vector/tensor values of solution fields probed at a query point  $\mathbf{x} \in \Omega_0$  are denoted by  $\mathbf{u}_\Omega(\mathbf{x}) = \mathcal{A}_1(\mathbf{x}; \Omega)$  and  $\sigma_\Omega(\mathbf{x}) = \mathcal{A}_2(\mathbf{x}; \Omega)$ . In this case, both functions are zero outside the design, i.e.,  $\mathcal{A}_{1,2}(\mathbf{x}; \Omega) = 0$  if  $\mathbf{x} \in (\Omega_0 - \Omega)$ . FEA solves the weak form of the governing differential equation, discretized into a linear system (e.g., using hat functions)  $[K_\Omega][\mathbf{u}_\Omega] = [\mathbf{f}]$ , where the stiffness matrix  $[K_\Omega]$  and external load vector  $[\mathbf{f}]$  depend on the design shape and material properties, as well as boundary conditions. The equations are solved to obtain the discrete form of the displacement field  $[\mathbf{u}_\Omega]$  from which the discrete form of the stress field  $[\sigma_\Omega]$  is computed by linear operations.

Another example is accessibility analysis for machining (e.g., milling or turning) [7, 13]. For instance, consider an FP-solver for 3-axis milling simulation, which computes (discretized forms of) a volumetric measure of inaccessibility as a field  $\mu_\Omega(\mathbf{x}) := \mathcal{A}_3(\Omega)$  for a given design  $\Omega \in \mathcal{D}$  and machine tool parameters. This measure at a query point  $\mathbf{x} \in \Omega_0$ , denoted by  $\mu_\Omega(\mathbf{x}) = \mathcal{A}_3(\mathbf{x}; \Omega)$ , returns the penetration volume of the moving tool assembly  $T = (H \cup C)$ , including the holder  $H$  and cutter  $C$ , into the stationary obstacles  $O_\Omega = (\Omega \cup F)$ , including target form  $\Omega$  and fixtures  $F$ . The solver computes the discrete form of this field (e.g., sampled at point clouds or voxels)  $[\mu_\Omega]$  as a convolution between the discrete forms of the indicator functions of stationary solids  $[\mathbf{1}_{O_\Omega}]$  and moving solids  $[\mathbf{1}_T]$  using a fast Fourier transform (FFT) [74]. The maximal set of accessible configurations – in this case, pure translations in 3D for a fixed orientation – is then obtained as the null set  $M_\Omega = \mu_\Omega^{-1}(0)$ , i.e., the translations that do not lead to undesirable collisions. The maximal removable volume is obtained by sweeping the cutter with the maximal motion, i.e.,  $R_\Omega := \text{sweep}(M_\Omega, C)$ . Its indicator function  $\mathbf{1}_{R_\Omega}(\mathbf{x}) = \mathcal{A}_4(\mathbf{x}; \Omega)$  can be viewed as a predicate for accessibility, i.e., it returns 1 (resp. 0) if the query point  $\mathbf{x} \in \Omega_0$  is (resp. is not) accessible. The discrete form of this binary field  $[\mathbf{1}_{R_\Omega}]$  can also be obtained by thresholding FFT-based convolution of discrete forms  $[\mathbf{1}_{M_\Omega}]$  and  $[\mathbf{1}_C]$ .

The computations performed by the above two FP-solvers (FEA and accessibility analysis) are abstracted by  $\mathcal{A} := (\mathcal{A}_1, \mathcal{A}_2, \mathcal{A}_3, \mathcal{A}_4)$  that maps a given design to a “field tuple” that represents analysis results. Figure 8 illustrates one instance of each such field for a topologically optimized bracket—solution of a DARPA design challenge problem for TRANSformative DESign (TRADES) program.

### 3.1.2. Feasible Design Subspaces & Predicates

Inverse problem solvers (IP-solvers), on the other hand, find one or more designs that satisfy a given collection of functional requirements. Most IP-solvers employ an iterative process to:

1. generate one or more valid candidate design(s);
2. perform analysis on the candidate design(s) to compute the performance(s) of interest (using one or more FP-solver(s));
3. evaluate the performance(s) against given functional requirements; and,
4. if the requirements are not met, decide on the next generation of candidate design(s) based on the current evaluation and update rules.

The process is repeated until the requirements are met. The evaluation process (item 3) can be conceptualized as finite number of predicates defined over the performance space as  $c_i : D \rightarrow \{0, 1\}$  for  $i = 1, 2, \dots, n$ . Each predicate's outcome  $c_i(\Omega) \in \{0, 1\}$  is determined by means of a *constraint* imposed on the performance field  $\mathcal{A}_i(\Omega) \in F_i$  simulated by an FP-solver:<sup>3</sup>

$$c_i(\Omega) := \begin{cases} 1 & \text{if the } i^{\text{th}} \text{ constraint is satisfied,} \\ 0 & \text{otherwise.} \end{cases} \quad (1)$$

These can be (in)equality constraints (Sections 3.2), which are common in physics-based design formulations as in TO, and set constraints (Section 3.3), which are ubiquitous in design under kinematics-based constraints such as packaging, assembly, and accessibility for manufacturing.

We can think of the performance criteria evaluation as a map  $\mathbf{c} := (c_1, c_2, \dots, c_n) : D \rightarrow \{0, 1\}^n$  i.e.,  $\mathbf{c}(\Omega)$  is a binary string whose bits indicate whether a given design satisfies each of the criteria (Fig. 8). A design  $\Omega \in D$  is called 'feasible' if it simultaneously satisfies all criteria, i.e.,  $\mathbf{c}(\Omega) = (1, 1, \dots, 1)$ . The *feasible design subspace*  $D^* \subseteq D$  is the subset of all feasible designs, defined as:

$$D^* := \{\Omega \in D \mid \mathbf{c}(\Omega) = \mathbf{1}^n\} =: \mathbf{c}^{-1}(\mathbf{1}). \quad (2)$$

Here,  $(\cdot)^{-1}$  denotes inversion of a mathematical relation.<sup>4</sup>

Unlike forward problems, inverse problems have non-unique, often infinitely many, solutions (i.e.,  $|D^*| > 1$ ). The feasible design space can also be defined as the intersection of the *feasibility halfspaces*  $H_i := c_i^{-1}(1)$ , each

implicitly describing one of the design subspaces that satisfy one criterion at-a-time:

$$D^* = \bigcap_{1 \leq i \leq n} c_i^{-1}(1) = D - \bigcup_{1 \leq i \leq n} c_i^{-1}(0). \quad (3)$$

The idea of design space pruning (Section 4) is to progressively cut out portions of the design space that violate any one of the criteria. Theoretically, pruning can be done in an arbitrary order—noting that intersections or unions of the halfspace in (3) are permutative. Computationally, however, it is only possible if the design subspaces  $H_i = c_i^{-1}(1)$  can be manipulated by algorithms as first-class entities. Our goal is to understand under what conditions such manipulations are possible and how an entire design subspace can be represented. The existence (Proposition 1) and completeness (Proposition 2) of such representations are discussed in Section 4.

### 3.2. Global, Local, & Strictly Local Inequality Constraints

The predicates introduced earlier are implemented in practice by testing whether a candidate design's performance satisfies an (in)equality constraint.<sup>5</sup> We classify such constraints into three types; namely, global, local, and strictly local (in)equality constraints.

#### 3.2.1. Global Inequality Constraints

It is common to have design criteria specified in terms of global constraints  $g_i(\Omega) \leq 0$ , i.e., by defining a predicate of the general form:

$$c_i(\Omega) := \begin{cases} 1 & \text{if } g_i(\Omega) \leq 0, \\ 0 & \text{otherwise.} \end{cases} \quad (4)$$

in which  $g_i : D \rightarrow \mathbb{R}$  is a function of the *entire* shape of the design  $\Omega \in D$ , potentially in addition to fixed external factors such as boundary conditions, manufacturing process parameters, packaging envelope, operating conditions (e.g., motion in assembly), etc. The constraint is often evaluated in terms of a global property of an entire performance field  $\mathcal{A}_i(\Omega) \in F_i$ , e.g., as an upper/lower-bound on its maximum/minimum or its integral properties such as  $p$ -norms. This is denoted by  $g_i(\Omega) = \bar{g}_i(\mathcal{A}_i(\Omega))$  where  $\bar{g}_i : D \rightarrow \mathbb{R}$ . For example, one can constrain the maximal displacement or maximal stress of a solid under external loads (Fig. 8) by using the following constraints in (4):

$$g_1(\Omega) = \bar{g}_1(\mathbf{u}_\Omega) := \max_{\mathbf{x} \in \Omega} \|\mathbf{u}_\Omega(\mathbf{x})\| - \delta_{\text{UB}}, \quad (5)$$

$$g_2(\Omega) = \bar{g}_2(\sigma_\Omega) := \max_{\mathbf{x} \in \Omega} \|\sigma_\Omega(\mathbf{x})\| - \sigma_{\text{UB}}, \quad (6)$$

where  $\delta_{\text{UB}}, \sigma_{\text{UB}} > 0$  are constant upper-bounds on the magnitude of the displacement vector and stress tensor, captured by the constraints  $g_1(\Omega) \leq 0$  and  $g_2(\Omega) \leq 0$ ,

<sup>3</sup>Without loss of generality, we assume that every requirement depends on one performance field only. If more than one field is used in calculating a predicate, we tuple those fields into another field. If more than one requirement is computed on one field, we think of it as two copies of the same field.

<sup>4</sup>Given  $f : X \rightarrow Y$ , we define  $f^{-1}(y) = \{x \in X \mid f(x) = y\}$ . Note that in general,  $f^{-1}(y) \subseteq X$  is a set, i.e.,  $f^{-1} : Y \rightarrow \mathcal{P}(X)$ . It is a singleton set (i.e., has one element) if the function is bijective.

<sup>5</sup>Note that every equality constraint  $g(\cdot) = 0$  can be represented by two inequality constraints  $g(\cdot) \leq 0$  and  $-g(\cdot) \leq 0$ .



respectively. One can in general use the  $p$ -norm of the fields for finite (but large)  $p \geq 1$ , noting that maximum is a special case as  $p \rightarrow \infty$ . This is especially useful to smooth out the possible singularities (e.g., infinite stress, due to stress concentrations).

Here is another example to constrain a design to be manufacturable via machining, using the accessibility analysis mentioned earlier:

$$g_3(\Omega) = \bar{g}_3(\mathbf{1}_{R_\Omega}) := \int_{\Omega_0 - \Omega} -\mathbf{1}_{R_\Omega}(\mathbf{x}) \, dv[\mathbf{x}] - V_{\text{UB}}, \quad (7)$$

where  $-\mathbf{1}_{R_\Omega}(\mathbf{x}) = 1 - \mathbf{1}_{R_\Omega}(\mathbf{x})$  is a negation. This constraint restricts the total volume of inaccessible regions  $R_\Omega \subseteq \Omega^c$ , obtained as the 1-norm of their indicator function, by an upper-bound  $V_{\text{UB}} > 0$ .

### 3.2.2. Local Inequality Constraints

It is sometimes possible to define a predicate in terms of local constraints evaluated at a specific point in the design domain; for instance, using one of the following forms:

$$c_i(\Omega) := \begin{cases} 1 & \text{if } \forall \mathbf{x} \in \Omega_0 : g_i(\mathbf{x}; \Omega) \leq 0, \\ 0 & \text{otherwise.} \end{cases} \quad (8)$$

$$c_i(\Omega) := \begin{cases} 1 & \text{if } \exists \mathbf{x} \in \Omega_0 : g_i(\mathbf{x}; \Omega) \leq 0, \\ 0 & \text{otherwise.} \end{cases} \quad (9)$$

Note that the two alternative forms are different by the “for all” and “there exists” quantifiers, which lead to different global implications. Unlike the case with (4), here  $g_i : (\Omega_0 \times \mathcal{D}) \rightarrow \mathbb{R}$  is field for a fixed design  $\Omega \in \mathcal{D}$ , i.e., is also a function of the query point  $\mathbf{x} \in \Omega_0$ . In turn, the constraint is evaluated based on the probed *value* of the performance field  $\mathcal{A}_i(\mathbf{x}; \Omega) \in \mathbb{Q}_i$  (generally, a tensor) at the query point. We denote this dependency by  $g_i(\mathbf{x}; \Omega) = \bar{g}_i(\mathcal{A}_i(\mathbf{x}; \Omega))$  where  $\bar{g}_i : \mathbb{Q}_i \rightarrow \mathbb{R}$ . For example, the global displacement and stress bounds mentioned earlier can be imposed locally (Fig. 8):

$$g_1(\mathbf{x}; \Omega) = \bar{g}_1(\mathbf{u}_\Omega(\mathbf{x})) := \|\mathbf{u}_\Omega(\mathbf{x})\| - \delta_{\text{UB}}, \quad (10)$$

$$g_2(\mathbf{x}; \Omega) = \bar{g}_2(\sigma_\Omega(\mathbf{x})) := \|\sigma_\Omega(\mathbf{x})\| - \sigma_{\text{UB}}, \quad (11)$$

It is easy to verify that using (10) and (11) with (8) is equivalent to using (5) and (6) with (4) in this example. In general, local constraints  $g_i(\mathbf{x}; \Omega) \leq 0$  used with “for all” or “there exists” quantifiers in (8) and (9) can be equivalently expressed as global constraints (stated independently of  $\mathbf{x} \in \Omega_0$ ) via min/max, respectively:

$$\left[ \forall \mathbf{x} \in \Omega_0 : g_i(\mathbf{x}; \Omega) \leq 0 \right] \Leftrightarrow \max_{\mathbf{x} \in \Omega_0} g_i(\mathbf{x}; \Omega) \leq 0, \quad (12)$$

$$\left[ \exists \mathbf{x} \in \Omega_0 : g_i(\mathbf{x}; \Omega) \leq 0 \right] \Leftrightarrow \min_{\mathbf{x} \in \Omega_0} g_i(\mathbf{x}; \Omega) \leq 0. \quad (13)$$

As another example, consider the accessibility analysis discussed earlier. Instead of constraining the total volume of inaccessible regions via the global constraint of (7), we can locally constrain the inaccessibility measure as:

$$g_4(\mathbf{x}; \Omega) = \bar{g}_4(\mu_\Omega(\mathbf{x})) := (\mathbf{1}_{O_\Omega} * \mathbf{1}_{-T})(\mathbf{x}) - \mu_0, \quad (14)$$

where  $O_\Omega = (\Omega \cup F)$  and  $T = (H \cup C)$  are the stationary and moving solids, respectively.  $\mu_0 > 0$  is a small constant to provide allowance for numerical errors. The convolution operator  $*$  is defined as:

$$(\mathbf{1}_{O_\Omega} * \mathbf{1}_{-T})(\mathbf{x}) = \int_{\Omega_0} \mathbf{1}_\Omega(\mathbf{x}') \mathbf{1}_{-T}(\mathbf{x} - \mathbf{x}') \, dv[\mathbf{x}'], \quad (15)$$

where  $\mathbf{1}_{-T}(\mathbf{x}) = \mathbf{1}_T(-\mathbf{x})$  is a reflection with respect to the origin, hence  $\mathbf{1}_{-T}(\mathbf{x} - \mathbf{x}') = \mathbf{1}_T(\mathbf{x}' - \mathbf{x})$  is the indicator function of the moving object (i.e., tool assembly), translated to the query point  $\mathbf{x} \in \Omega_0$ . The integral is nonzero at integration points  $\mathbf{x}' \in \Omega_0$  that belongs to the interference of the translated object with the stationary obstacles.

It is not always possible to convert global constraints to local constraints or vice versa, without defining new performance variables, e.g., in terms of the norms of existing performance fields. We show in the next section that when  $\mathcal{A}_i(\mathbf{x}; \Omega)$  is decidable independently of  $\Omega \in \mathcal{D}$ , the above two constraints lead to maximal/minimal feasible designs (in set-theoretic terms).

### 3.2.3. Strictly Local Inequality Constraints

An important special case of (8) occurs if the predicate is *decidable without a priori knowledge of the design itself*. In other words, the constraints can be evaluated purely from a knowledge of the query point’s position  $\mathbf{x} \in \Omega$  and external factors, if any (e.g., a known rigid body motion applied to the entire design). The predicate’s result can be obtained without knowing the overall shape of the design. This is the case if  $\mathcal{A}_i(\mathbf{x}; \Omega) = \mathcal{A}_i^*(\mathbf{x})$ , i.e., the forward problem’s solution can be evaluated pointwise—emphasized by the overline notation. The corresponding constraint  $\bar{g}_i^*(\mathbf{x}) := \bar{g}_i(\mathcal{A}_i^*(\mathbf{x})) \leq 0$  is hereafter called a *strictly local* (i.e., pointwise) constraint. The predicates in (8) or (9) in this case are dependent on  $\Omega$  only due to the logical quantifiers for the pointwise testing:

$$c_i(\Omega) := \begin{cases} 1 & \text{if } \forall \mathbf{x} \in \Omega : \bar{g}_i^*(\mathbf{x}) \leq 0, \\ 0 & \text{otherwise.} \end{cases} \quad (16)$$

$$c_i(\Omega) := \begin{cases} 1 & \text{if } \exists \mathbf{x} \in \Omega : \bar{g}_i^*(\mathbf{x}) \leq 0, \\ 0 & \text{otherwise.} \end{cases} \quad (17)$$

Hence, one can define *pointwise predicates* in this case:

$$c_i^*(\mathbf{x}) := \begin{cases} 1 & \text{if } \bar{g}_i^*(\mathbf{x}) \leq 0, \\ 0 & \text{otherwise.} \end{cases} \quad (18)$$

We show in Section 4 that the pointwise predicate defines a point membership classification (PMC) that implicitly determines the entire feasibility halfspace  $\mathbf{H}_i = c_i^{-1}(1)$  using its “representative” maximal/minimal feasible design  $\Omega_i^* := c_i^{*-1}(1)$  using (16) or (17), respectively. In this paper, we restrict our attention to the former (“for all” quantifier and maximal designs), since it lends itself to material reducing downstream solvers such as TO.

The physics-based constraints exemplified earlier might reduce to pointwise constraints in rare examples—e.g., the stress tensor  $\sigma^*(\mathbf{x})$  for hydrostatic pressure in a liquid container at rest depends on the query point’s depth from the surface, but not on the container’s designed shape. Nevertheless, pointwise constraints are ubiquitous in kinematics-based constraints that are central to applications ranging from assembly and packaging to manufacturing. In the next section, we present an important subclass of pointwise constraints that manifest as *set constraints*.

### 3.3. Converting Set Constraints to Inequality Constraints

Many kinematics-based design criteria lead to constraints expressed in the algebra of sets. A common form of set constraints is in terms of *containment*:  $\Gamma(\Omega) \subseteq E$  (for a fixed envelope  $E \subseteq \mathbb{R}^d$ ). The exact same constraint can be written in terms of *non-interference*:  $(\Gamma(\Omega) \cap O) = \emptyset$  (for a fixed obstacle  $O \subseteq \mathbb{R}^d$ ), where  $\Gamma : \mathcal{D} \rightarrow \mathcal{P}(\mathbb{R}^d)$  is a *set transformation* and  $E := O^c$  (i.e., complement of  $O$ ).

At a first glance, these constraints appear to have a completely different form than the inequality constraints described in Section 3.2 in the algebra of fields. Here, we show that set constraints can *always* be reformulated as (global or local) inequality constraints by virtue of describing sets with their indicator functions. However, converting them to strictly local (i.e., pointwise) constraints is possible under certain conditions.

#### 3.3.1. Global or Local Set Constraints

For every solid  $\Omega \in \mathcal{D}$ , its indicator (i.e., characteristic) function  $\mathbf{1}_\Omega : \Omega_0 \rightarrow \{0, 1\}$  is defined as:

$$\mathbf{1}_\Omega(\mathbf{x}) := \begin{cases} 1 & \text{if } \mathbf{x} \in \Omega, \\ 0 & \text{otherwise.} \end{cases}, \text{ i.e., } \Omega = \mathbf{1}_\Omega^{-1}(1). \quad (19)$$

Hence, every containment constraint is restated as an inequality constraint of the form used in (8):

$$\Gamma(\Omega) \subseteq E \iff \left[ \forall \mathbf{x} \in \mathbb{R}^d : \mathbf{1}_{\Gamma(\Omega)}(\mathbf{x}) \leq \mathbf{1}_E(\mathbf{x}) \right], \quad (20)$$

i.e., using the standard form  $\mathbf{1}_{\Gamma(\Omega)}(\mathbf{x}) - \mathbf{1}_E(\mathbf{x}) \leq 0$ .

Recall from Section 3.2 that the above inequality constraint can also be rewritten as a global constraint of the form used in (4) by upper-bounding the maximum:

$$\Gamma(\Omega) \subseteq E \iff \max_{\mathbf{x} \in \mathbb{R}^d} [\mathbf{1}_{\Gamma(\Omega)}(\mathbf{x}) - \mathbf{1}_E(\mathbf{x})] \leq 0, \quad (21)$$

Notice that we have not made any assumption on the properties of the pointsets  $\Gamma(\Omega), E \subseteq \mathbb{R}^d$ . In most practical scenarios, both are solids within a bounded domain, taken as the design domain  $\Omega_0 \in \mathcal{D}$ . In such cases, the properties of the mapping and envelope can be exploited to compute the maximum in (21) efficiently.

Moreover, if the set constraint  $(\Gamma(\Omega) \cap E^c) = \emptyset$  is in terms of regularized intersection, it can be rewritten as a global (in)equality constraint in terms of the volume

$\text{vol}(\Gamma(\Omega) \cap E^c) = 0$  (or  $\leq 0$ , for consistency), which, in turn, is an inner product of indicator functions:

$$\text{vol}[\Gamma(\Omega) \cap E^c] = \langle \mathbf{1}_{\Gamma(\Omega)}, \neg \mathbf{1}_E \rangle \quad (22)$$

$$= \int_{\mathbb{R}^d} \neg \mathbf{1}_{\Gamma(\Omega)}(\mathbf{x}) \mathbf{1}_E \, dv[\mathbf{x}]. \quad (23)$$

Further, if  $\Gamma(\Omega)$  is a rigid transformation of  $\Omega$ , the inner product turns into a *convolution* of  $\mathbf{1}_\Omega$  and  $\neg \mathbf{1}_E$  over the configuration space of motions [65].

Let us consider the inaccessibility analysis one more time. For manufacturing with precision requirements (e.g., for assembly/fit), we can restrict the inaccessible regions  $\Gamma(\Omega) := (\Omega_0 - \Omega) - R_\Omega$  to be completely contained within a tolerance zone  $E \subseteq \mathbb{R}^d$ , hence formulating the problem as a set constraint  $\Gamma(\Omega) \subseteq E$ , where:

$$\Gamma(\Omega) = (\Omega_0 - \Omega) - \text{sweep}(M_\Omega, C). \quad (24)$$

For translational motions  $M_\Omega \subseteq \mathbb{R}^d$ , the sweep in (24) can be simplified into a Minkowski sum:

$$\Gamma(\Omega) = (\Omega_0 - \Omega) - (M_\Omega \oplus C). \quad (25)$$

The maximal collision-free motion [7] is obtained as the complement of the  $\mathcal{C}$ -space obstacle, which is in turn computed by Minkowski operations (for translational full-dimensional motions):<sup>6</sup>

$$\Gamma(\Omega) = (\Omega_0 - \Omega) - ((\Omega \oplus (-T))^c \oplus C) \quad (26)$$

$$= (\Omega_0 - \Omega) - ((\Omega^c \ominus (-T)) \oplus C), \quad (27)$$

where  $T = (H \cup C)$  represents the tool assembly, including the holder  $H$  and the cutter  $C$ . It is understood that Minkowski sums in (26) can be obtained from the 0-superlevel set of the convolution fields of the participating sets [65].<sup>7</sup> More precisely:

$$\mathbf{1}_{\Gamma(\Omega)} = \neg \mathbf{1}_\Omega - \text{sign}(-\text{sign}(\mathbf{1}_\Omega * \mathbf{1}_{-T}) * \mathbf{1}_C), \quad (28)$$

where  $*$  is the convolution operator in  $\mathbb{R}^d$  and  $\text{sign}(x) = 1$  (resp. 0) if  $x > 0$  (resp.  $x \leq 0$ ) is the sign function. The latter is needed to convert the real-valued convolutions to binary-valued indicator functions. See [65] for a proof.

In summary, set constraints, as defined in this section in terms of containment or non-interference, can *always* be restated as global or local inequality constraints defined in Section 3.2. In the next section, we show the conditions under which set constraints can be converted to strictly local (i.e., pointwise) constraints, to enable design space pruning in Section 4.

<sup>6</sup>The operators  $(\cdot)^c, \cup, \cap, -, \oplus, \ominus$  are all regularized to ensure their algebraic closure within the design space  $\mathcal{D}$  [75]. The caveat is that collision-free lower-dimensional motions (e.g., of a peg inside a hole with no clearance) would be pruned from collision-free motions.

<sup>7</sup>In general,  $Y = (X_1 \oplus X_2) \iff \mathbf{1}_Y = \text{sign}(\mathbf{1}_{X_1} * \mathbf{1}_{X_2})$  [65].

### 3.3.2. Set Constraints as Pointwise Constraints

Depending on the properties of  $\Gamma : \mathcal{D} \rightarrow \mathcal{P}(\mathbb{R}^d)$ , the inequality constraint  $\mathbf{1}_{\Gamma(\Omega)}(\mathbf{x}) - \mathbf{1}_E(\mathbf{x}) \leq 0$ , used in global or local forms of (20) and (21), respectively, may or may not be restated as a strictly local (i.e., pointwise) constraint. Our goal in this section is to articulate the conditions under which this is possible.

To enable pointwise formulation, we need to eliminate the dependency of the PMC for  $\Gamma(\Omega)$  on  $\Omega$  so that  $\mathbf{1}_{\Gamma(\Omega)}(\mathbf{x})$  on the left-hand side of the inequality constraint in (20) depends only on the query point  $\mathbf{x} \in \Omega_0$  and the fixed envelope  $E \subseteq \mathbb{R}^d$ . This can be done if the set transformation  $\Gamma$  is itself a pointwise transformation, meaning that it can be defined by *extending* a transformation of 3D points  $\gamma : (\mathbb{R}^d \text{ or } \Omega_0) \rightarrow \mathcal{P}(\mathbb{R}^d)$  to a transformation of 3D pointsets  $\Gamma : \mathcal{D} \rightarrow \mathcal{P}(\mathbb{R}^d)$  by simply applying the former to every point of the pointset and unifying the results:

$$\Gamma(\Omega) := \bigcup_{\mathbf{x} \in \Omega} \gamma(\mathbf{x}) = \{\mathbf{x}' \mid \mathbf{x}' \in \gamma(\mathbf{x}), \mathbf{x} \in \Omega\}. \quad (29)$$

Note that  $\gamma(\mathbf{x})$  is itself a pointset, not a point, to capture the most general case. For example, it can be a curve segment or surface patch representing the 1D or 2D trajectory of a point under a given one- or two-parametric motion, respectively.

The above refactoring is possible for many important applications. For example, if the design has to move (when deployed in assembly) according to a known motion set  $M \subseteq \text{SE}(3)$  without exiting a safe region of space  $E \subseteq \mathbb{R}^d$  that contains no obstacles [14], the above constraint can be used with  $\Gamma(\Omega) := \text{sweep}(M, \Omega)$ , where

$$\text{sweep}(M, \Omega) = \bigcup_{\tau \in M} \tau\Omega = \{\tau\mathbf{x} \mid \tau \in M, \mathbf{x} \in \Omega\}, \quad (30)$$

is the sweep of the designed part as it travels by the given motion (known a priori). In this case the sweep indicator function  $\mathbf{1}_{\Gamma(\Omega)}$  can be directly obtained as follows:

$$\mathbf{1}_{\Gamma(\Omega)}(\mathbf{x}) = 1 \text{ iff } \exists \tau \in M : \mathbf{x} \in \tau\Omega, \text{ i.e., } \tau^{-1}\mathbf{x} \in \Omega, \quad (31)$$

In other words, a PMC test for  $\Gamma(\Omega)$  can be obtained by applying the inverse motion  $M^{-1} = \{\tau^{-1} \mid \tau \in M\}$  to the query point and checking if it intersects the design. The inequality constraint in (21) can thus be computed rapidly by sampling query points in the design domain and testing intersections of their inverse trajectories with the design [14]. Importantly, the computation for one point does *not* need one to have explicit knowledge of the results for other points. Other than perfect parallelization (e.g., on GPU), this property enables pruning the design space – leading to development of the `Un sweep` solver discussed earlier – before optimizing the design for other criteria.

In general, for pointwise transformations as in (29), the global constraint  $\Gamma(\Omega) \subseteq E$  can be restated as:

$$\Gamma(\Omega) \subseteq E \iff \left[ \forall \mathbf{x} \in \Omega : \gamma(\mathbf{x}) \subseteq E \right], \quad (32)$$

i.e.,  $\Omega$  remains within  $E$  after a  $\Gamma$ -transform iff all points inside it remain within  $E$  after a  $\gamma$ -transform. Note also that inequality constraint in (20) can now be rewritten in a pointwise fashion every  $\mathbf{x} \in \Omega$ :

$$\forall \mathbf{x} \in \Omega : \forall \mathbf{x}' \in \mathbb{R}^d : \mathbf{1}_{\gamma(\mathbf{x})}(\mathbf{x}') \leq \mathbf{1}_E(\mathbf{x}'), \quad (33)$$

As with other inequality constraints, not every global or local set constraint can be converted to a pointwise set constraint. For example, the toleranced accessibility constraints  $\Gamma(\Omega) \subseteq E$  for  $\Gamma(\Omega) := (\Omega_0 - \Omega) - \text{sweep}(M_\Omega, C)$  in (24) cannot be evaluated pointwise, because the maximal collision-free motion  $M_\Omega = (\Omega \oplus (-T))^c$  depends on the global shape of  $\Omega$ , unlike the case with the fixed motion in the earlier example with `Un sweep`.

### 3.4. Design for Heterogeneous Constraints

We conclude this section by a fairly general formulation of a design problem subject to  $n \geq 1$  heterogeneous (e.g., kinematics- and physics-based) constraints.

Without loss of generality, let  $n_C = n_G + n_L + n_P$  where  $0 \leq n_G, n_L, n_P \leq n_C$  are the number of global, local, and strictly local (i.e., pointwise) constraints, respectively. All constraints, including set constraints, are expressed as inequality constraints for uniformity. The *design problem* is to identify the feasible design space  $\mathcal{D}^* = \mathcal{c}^{-1}(1)$ , stated as a constraint satisfaction problem:

$$\begin{aligned} \text{Find } \mathcal{D}^* \subseteq \mathcal{D}, \text{ such that for all } \mathbf{x} \in \Omega \in \mathcal{D}^* : \\ g_i^*(\mathbf{x}) &\leq 0, \quad \text{for } 0 < i \leq n_P, \\ g_i(\Omega) &\leq 0, \quad \text{for } n_P < i \leq n_P + n_G, \\ g_i(\mathbf{x}; \Omega) &\leq 0, \quad \text{for } n_P + n_G < i \leq n_C, \end{aligned} \quad (34)$$

We assume that none of the  $g_i(\mathbf{x}; \Omega) \leq 0$  can be simplified into one of  $g_i^*(\mathbf{x}) \leq 0$  or  $g_i(\Omega) \leq 0$  forms. Hereafter, we use the P-, G-, and L-subscripts for various notions related to pointwise, global, and local constraints, respectively; for instance,  $\mathcal{D}^* = \mathcal{D}_P^* \cap \mathcal{D}_G^* \cap \mathcal{D}_L^*$  where  $\mathcal{D}_P^* = \mathcal{c}_P^{-1}(1)$  is the design subspace that is feasible with respect to pointwise constraint alone, and so on. We solve the design problem in two phases, depicted in Fig. 7 (b):

**Phase 1.** Prune the design space from  $\mathcal{D}$  to  $\mathcal{D}_P^* = \mathcal{c}_P^{-1}(1)$ , i.e., solve the following (simpler) problem:

$$\begin{aligned} \text{Find } \mathcal{D}_P^* \subseteq \mathcal{D}, \text{ such that for all } \mathbf{x} \in \Omega \in \mathcal{D}_P^* : \\ g_i^*(\mathbf{x}) \leq 0, \quad \text{for } 0 < i \leq n_P. \end{aligned} \quad (35)$$

In Section 4, we solve the above problem by computing a maximal set  $\Omega_P^* := \max \mathcal{D}^*$  in the partial ordering of designs via set containment.

Unfortunately, this is not possible for  $\mathcal{D}_G^*$  and  $\mathcal{D}_L^*$ . In most cases, one can at best generate a finite sample of feasible designs that are superior in some way.

**Phase 2.** Explore the pruned design space  $D_P^*$  to find a sample  $D_{\text{dom}}^* \subset D^*$  of (locally) “Pareto-dominant” [24, 25] designs that satisfy the remaining constraints:

$$\begin{aligned} &\text{Find } D_{\text{dom}}^* \subset D_P^*, \text{ such that for all } \mathbf{x} \in \Omega \in D_{\text{opt}}^* : \\ &g_i(\Omega) \leq 0, \quad \text{for } n_P < i \leq n_P + n_G, \\ &g_i(\mathbf{x}; \Omega) \leq 0, \quad \text{for } n_P + n_G < i \leq n_C, \end{aligned} \quad (36)$$

Pareto-dominance of  $\Omega \in D_{\text{dom}}^*$  means that for some neighborhood  $N(\Omega) \subseteq D_P^*$  and  $\Omega \in N(\Omega)$  in the pruned design space,<sup>8</sup> within which no other design is superior to  $\Omega$  with respect to all objective functions  $f_1, f_2, \dots, f_{n_O} : D \rightarrow \mathbb{R}$ . We can pose this as a minimization problem:

$$\text{Find } \Omega \in D_P^* \text{ to } \begin{cases} \text{minimize } f_j(\Omega), \text{ for } 0 < j \leq n_O, \\ \text{subject to constraints in (36)}. \end{cases} \quad (37)$$

The objective functions define another partial ordering over the pruned design space, whose maximal elements we seek, i.e.,  $D_{\text{dom}}^* := \max D$ .

In Section 5, we solve the above problem by iterative optimization guided by TSF. The TSF is defined with respect to global objective functions  $f_j(\Omega)$  and global constraints  $g_i(\Omega) \leq 0$  and is penalized/filtered using local constraints  $g_i(\mathbf{x}; \Omega) \leq 0$ . Since global optimization ( $N(\Omega) := D_P^*$ ) is NP-hard [23], we settle for local optimality.

## 4. Design Space Pruning

In this section, we present a methodology to solve the **phase 1** problem formulated in (35) of Section 3.4. Using the terminology and results of Section 3, we show how the design space can be pruned with respect to pointwise constraints (including set constraints) without premature optimization. We illustrate the process using examples from kinematics-based constraints that are common in assembly, packaging, and manufacturing.

### 4.1. Existence & Completeness of Maximal Designs

The following results on the existence and uniqueness of maximal pointsets and their informational completeness as a representation for entire feasible design spaces are central to design space pruning.

**Proposition 1.** (Existence and Uniqueness) For every strictly local (i.e., pointwise) constraint  $g_i^*(\mathbf{x}) \leq 0$ , its feasibility halfspace  $H_i$  has a maximal element  $\Omega_i^* = \max H_i$ , defined implicitly by the following PMC test:

$$\mathbf{1}_{\Omega_i^*}(\mathbf{x}) := \begin{cases} 1 & \text{if } g_i^*(\mathbf{x}) \leq 0, \\ 0 & \text{otherwise,} \end{cases} \quad (38)$$

$$\text{i.e., } \Omega_i^* := \{\mathbf{x} \in \Omega_0 \mid g_i^*(\mathbf{x}) \leq 0\}. \quad (39)$$

The maximality is in terms of set containment, i.e., every satisfactory design is contained in the maximal element:  $\Omega \in H_i \Rightarrow \Omega \subseteq \max H_i$ .

<sup>8</sup>Technically,  $N(\Omega)$  is an open set in the induced Hausdorff topology of  $D_P^* = \mathcal{P}^*(\Omega^*)$  (all solid subsets of the maximal element).

**Proposition 2.** (Completeness) For every strictly local (i.e., pointwise) constraint  $g_i^*(\mathcal{A}_i(\mathbf{x})) \leq 0$ , its feasibility halfspace  $H_i$  contains every solid  $\Omega \subseteq \Omega_i^* = \max H_i$ , i.e., every solid subset of the maximal element is also feasible:  $\Omega \subseteq \max H_i \Rightarrow \Omega \in H_i$ .

In terms of predicates, the design subspace  $H_i = c_i^{-1}(1)$  (which satisfies (16)) can now be represented by a single design  $\Omega_i^* = \bar{c}_i^{-1}(1)$  (whose *all points* satisfy (18)). The maximal solid is thus a *complete* representation of the feasibility halfspace as the collection of all of its solid subsets denoted by  $H_i = \mathcal{P}^*(\Omega_i^*)$ .

Here is an intuitive but simplified reasoning:

1. The set  $\Omega_i^*$  defined by (38) or (39) contains all points that satisfy the constraints.
2. Every solid subset  $\Omega \subseteq \Omega_i^*$  of the maximal set satisfies the constraint, because all of its points satisfy the constraint independently of the global shape.
3. Conversely, every feasible solid  $\Omega \in H_i$  is the subset of  $\Omega_i^*$ , because it only includes points that satisfy this constraint independently of the global shape.

Note that the constraint’s independence of the shape of  $\Omega$  is crucial for this to hold. For global or local constraints with dependency on  $\Omega$  itself, attempting to write a PMC similar to (38) leads to a circular definition where the right-hand side depends on the set itself. For example, the (global or local) constraints given in Sections 3.2.1 and 3.2.2 on FEA and printability analyses do not lead to maximal elements because their constraints  $g_i(\mathcal{A}_i(\mathbf{x}; \Omega)) \leq 0$  depend on particular design instances. It does make sense to define the maximal set of a feasible space (e.g., using the set-builder definition in (39)) in a way that it depends on a particular instance of that space. On the other hand, the set constraints of Section 3.3.2, such as containment under a prescribed motion, do give rise to maximal elements, as we elaborate with examples in the following sections.

The above reasoning does not take topological regularization into account—there is no reason for a maximal set obtained via (38) or (39) to be a solid, hence it may not itself be a valid design. However, we show that there always exists a valid maximal element obtained by regularizing (38) or (39). The correct definition is:

$$\Omega_i^* := \text{ki}\{\mathbf{x} \in \Omega_0 \mid g_i^*(\mathbf{x}) \leq 0\}. \quad (40)$$

where  $k$  and  $i$  are the topological closure and interior operators, respectively.

**Proposition 3.** (Design Space Pruning) Given a number of pointwise constraints  $g_i^*(\mathbf{x}) \leq 0$  for  $i = 1, 2, \dots, n_P$ , the feasible design space  $D^*$ , defined by intersecting all feasibility halfspaces  $H_i^*$ , has a maximal element  $\Omega_P^* = \max D_P^*$  that satisfies the uniqueness and completeness properties, i.e.,  $\Omega \subseteq D_P^* \Rightarrow \Omega \in \Omega_P^*$ . It can be obtained by intersecting all maximal elements  $\Omega_i^* = \max H_i$ :

$$\Omega_P^* = \bigcap_{1 \leq i \leq n_P} \Omega_i^*, \quad \text{i.e., } \mathbf{1}_{\Omega_P^*}(\mathbf{x}) = \bigwedge_{1 \leq i \leq n_P} \mathbf{1}_{\Omega_i^*}(\mathbf{x}), \quad (41)$$

in which the intersection/conjunction operators need to be regularized.

To see why this is true, note that any query point's membership in an (unknown) feasible design can be tested against all  $m$  constraints independently of other points' membership. If  $g_i^*(\mathbf{x}) \leq 0$  for  $i = 1, 2, \dots, n_P$ , the point can (but does not have to) be included in the design, for it to be feasible. The feasible design is hence a subset of all points that satisfy all pointwise constraints.

*The above result enables computing on design subspaces as first-class objects. Computationally, the feasibility halfspaces are represented uniquely by their maximal elements. The pruning of halfspaces (abstract operation) is implemented by intersecting maximal elements, i.e., conjuncting point membership tests defined by pointwise constraints (concrete algorithm) in an arbitrary order.*

$$\begin{array}{ccc}
 D; H_1, H_2, \dots, H_{n_P} & \xrightarrow[\text{(Not directly computable)}]{\cap} & D_P^* \\
 \uparrow \mathcal{P}^* \text{ max} & & \uparrow \mathcal{P}^* \text{ max} \\
 \Omega_0; \Omega_1^*, \Omega_2^*, \dots, \Omega_{n_P}^* & \xrightarrow{\cap} & \Omega_P^*
 \end{array} \quad (42)$$

Figure 9 illustrates design space pruning via (3).

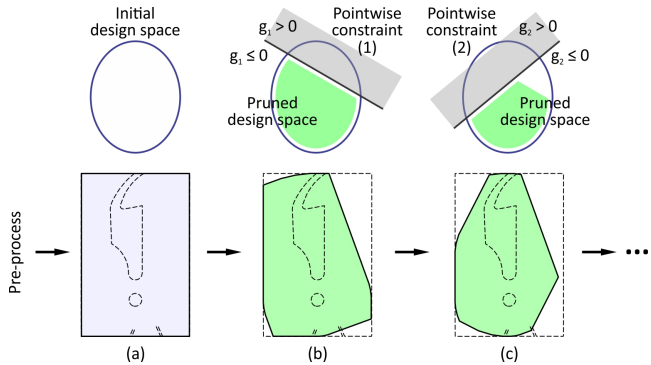


Figure 9: Design space pruning can be abstracted by intersecting the design space with feasibility halfspaces. This is not a computable operation in general. However, for pointwise constraints, it can be computed by intersecting maximal elements in the physical space.

Next, we consider maximal elements for set constraints in Section 4.2, and provide examples from real-world engineering problems in Section 4.3, 4.4, and 4.5.

#### 4.2. Maximal Pointsets for Set Constraints

Many design requirements, especially those that relate the interaction of moving shapes, may be expressed as set constraints of the form  $\Gamma(\Omega) \subseteq E$ , where  $\Gamma : D \rightarrow \mathcal{P}(\mathbb{R}^3)$  is a set transformation. For example,

- In packaging and assembly problems, the part's shape is often designed so that it is restricted to remain within a specified envelope while moving according to a prescribed motion.

- When designing part to be machined using a given tool that moves in the presence of obstacles (e.g., the part itself and fixtures), the surface of the part has to be accessible without collisions with the obstacles.

We will address examples of these problems in the following sections. The common theme to many motion-based set transformation  $\Gamma : D \rightarrow \mathcal{P}(\mathbb{R}^3)$  is that they can re-factored via (29) via a pointwise transformation  $\gamma : \Omega_0 \rightarrow \mathcal{P}(\mathbb{R}^3)$  that depends on the motion. The maximal pointset that satisfies the containment  $\Gamma(\Omega) \subseteq E$  or non-interference test  $(\Gamma(\Omega) \cap E^c) = \emptyset$  is defined implicitly by its PMC given in terms of  $\gamma$ :

$$\mathbf{1}_{\Omega_i^*}(\mathbf{x}) := \begin{cases} 1 & \text{if } \gamma(\mathbf{x}) \subseteq E, \\ 0 & \text{otherwise,} \end{cases} \quad (43)$$

$$\text{i.e., } \Omega_i^* := \{\mathbf{x} \in \Omega_0 \mid \gamma(\mathbf{x}) \subseteq E\} \quad (44)$$

$$= \gamma^{-1}(E) \cap \Omega_0, \quad (45)$$

where the set operators are regularized, as before. Note that  $\gamma^{-1}$  may not be a function, because  $\gamma$  is not necessarily invertible (see footnote 4).

Here are a few classical examples from solid modeling:

- For one-parametric sweep  $\Gamma(\Omega) := \text{sweep}(M, \Omega)$ , one has  $\gamma(\mathbf{x}) = M\mathbf{x}$  where  $M = M(t) \in \text{SE}(3)$  is a continuous one-parametric set of motions for  $t \in [t_{\min}, t_{\max}]$ . The maximal shape that satisfies  $\Gamma(\mathbf{x}) \subseteq E$  is given by an unsweep  $\text{unsweep}(M, E)$  [19].
- For Minkowski sum  $\Gamma(\Omega) := (\Omega \oplus B)$ , one has  $\gamma(\mathbf{x}) = (\mathbf{x} + B)$  where  $B \subset \mathbb{R}^3$  is typically a solid. The maximal shape that satisfies  $\Gamma(\mathbf{x}) \subseteq E$  is given by a Minkowski difference with  $(E \ominus (-B))$  [76].
- For general dilation (which subsumes the above two) with general rigid motions, the maximal shape is given by general erosion [77].
- For non-rigid (but pointwise pre-determined) deformations, the maximal shape is obtained by its PMC in terms of the pointwise displacement function.

**Procedure.** Propositions 1 through 3 suggest a systematic procedure to *prune* the design space, i.e., reduce the design space  $D$  to  $D_P^* = D \cap (H_1 \cap H_2 \cap \dots \cap H_{n_P})$  for kinematic criteria expressed in terms of pointwise set constraints:

- **Step 0.** Initialize the feasible design space with the design domain, i.e., in algorithmic terms,  $\Omega_P^* \leftarrow \Omega_0$ .
- **Step 1.** Express the set constraint that outlines one of the conditions for a given design  $\Omega \in D$  to be feasible in the form  $\Gamma(\Omega) \subseteq E$ . Check if it can be restated as a pointwise constraint  $\gamma(\mathbf{x}) \subseteq E$  as in (32).
- **Step 2.** Formalize the forward problem in terms of the PMC test for the maximal element obtained from the pointwise constraint as prescribed by (43).

- **Step 3.** Invoke an IP-solver for the inverse problem, which computes (an exact or approximate representation of) the maximal element  $\Omega_i^*$  in (44).
- **Step 4.** Prune the design space by intersecting the maximal element  $\Omega_p^*$  obtained so far the new  $\Omega_i^*$ , i.e.,  $\Omega_p^* \leftarrow (\Omega_p^* \cap \Omega_i^*)$  is a smaller maximal element representing a pruned feasible subspace.
- Repeat **steps 1–4** for all pointwise set constraints.

Notice that the above procedure can be applied to different constraints via independent invocation of IP-solvers in an arbitrary order.

Importantly, the IP-solver in **step 3** can be implemented in two fundamentally different ways to obtain either an *implicit* representation (i.e., using PMC test in (43)) or an *explicit* representation (i.e., using inversion in (45)) of the maximal element:

- If we have access to an IP-solver that computes an explicit representation (e.g., B-rep) of the inverse transformation  $\gamma^{-1}(E)$ , we can directly intersect it (using any CAD kernel) with the design domain to obtain the maximal element as prescribed by (45).
- If we have access to a FP-solver that computes (explicitly or implicitly) the forward transformation  $\gamma(\mathbf{x})$  for a given query point  $\mathbf{x} \in \Omega_0$ , we can compute an approximate representation (e.g., point cloud or voxelization) of the maximal element by:
  1. sampling the design domain with a sufficiently dense set of query points;
  2. invoking the FP-solver to PMC-test them using (45); keep the ones that pass the test and discard the ones that do not; and
  3. (optional) use adaptive local re-sampling around the points that passed the test to obtain a better approximation.

Because of the independence of pointwise test, invocation of the FP-solver for different query points can be done with perfect parallelization.

Let us apply this procedure to a few examples.

#### 4.3. Pruning for Containment of Moving Parts

Consider the latch design problem introduced earlier in Section 1.2, where the goal is to design a car hood latch that remains within an envelope  $E \subseteq \Omega_0$  while moving according to a motion  $M \subseteq \text{SE}(3)$ .

**Step 1.** Every feasible latch design  $\Omega \in \mathcal{D}$  must satisfy the set constraint  $\Gamma(\Omega) \subseteq E$  where  $\Gamma(\Omega) := \text{sweep}(M, \Omega)$ ; i.e., the swept volume by the latch after being transformed by all configurations  $\tau \in M$  (including any combination of translations and rotations, parameterized or otherwise) remains within the envelope. The sweep is a pointwise

transformation, i.e., can be computed as the union of all  $\gamma(\mathbf{x}) := M\mathbf{x} = \bigcup_{\tau \in M} \tau\mathbf{x}$ , which represents the trajectory traced by the query point  $\mathbf{x} \in \Omega_0$  along the prescribed motion. Hence, the containment constraint be tested in a pointwise fashion by  $\gamma(\mathbf{x}) \subseteq E$ .

**Step 2.** Using the definitions in (43), we construct a PMC test for the maximal shape in the design space that satisfies this pointwise constraint:

$$\mathbf{1}_{\Omega_1^*}(\mathbf{x}) := \begin{cases} 1 & \text{if } \forall \tau \in M : \tau\mathbf{x} \in E, \\ 0 & \text{otherwise.} \end{cases} \quad (46)$$

The forward problem involves following the trajectory, either exactly or approximately (e.g., by sampling), and testing whether it remains entirely within the envelope.

**Step 3.** The dual properties of the FP- and IP-solvers (i.e., **Sweep** and **Un sweep**) [19] can be leveraged to construct an exact or approximate representation of  $\Omega_1^*$ , as illustrated in Fig. 10. If we have access to an **Un sweep** solver, we can directly compute  $\Omega_1^* = \text{unsweep}(M^{-1}, E) \cap \Omega_0$ . However, if we only have access to an efficient **Sweep** solver, we can still compute an approximate representation of  $\Omega_1^*$  using the PMC test in (46) for a sufficiently dense sample of query points and retaining the points whose forward trajectory remains within the envelope [14]:

$$\left[ \forall \tau \in M : \tau\mathbf{x} \in E \right] \Leftrightarrow \mathbf{x} \in \bigcap_{\tau \in M} \tau^{-1}(E), \text{ i.e.,} \quad (47)$$

$$\text{sweep}(M, \Omega) \subseteq E \Leftrightarrow \Omega \subseteq \text{unsweep}(M^{-1}, E). \quad (48)$$

The *invertibility* of rigid transformations  $M \mapsto M^{-1}$  is key to efficient direct implementation of **Un sweep**.

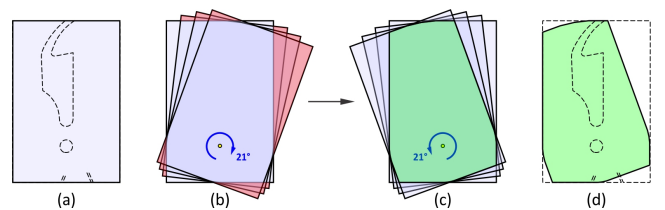


Figure 10:  $\text{unsweep}(R, E)$  is the largest set that remains within the square envelope  $E$  shown in (a) while moving by a  $21^\circ$  clockwise rotation  $R$  around a fixed pivot [14], i.e., without violating the containment constraint as depicted in red in (b). The unsweep can be computed in general by intersecting all moved instances of the envelope with an inverse motion [19].

The remaining **steps 4** and **5** are straightforward.

$\Omega_1^*$  can be sent as the initial design to design space exploration (Section 5) via TO or any other downstream material reducing IP-solver. It is guaranteed that every valid design  $\Omega \subseteq \Omega_1^*$  that is the output of the downstream IP-solver, no matter how complicated, will continue to satisfy the set constraint  $\text{sweep}(M, \Omega) \subseteq E$ .

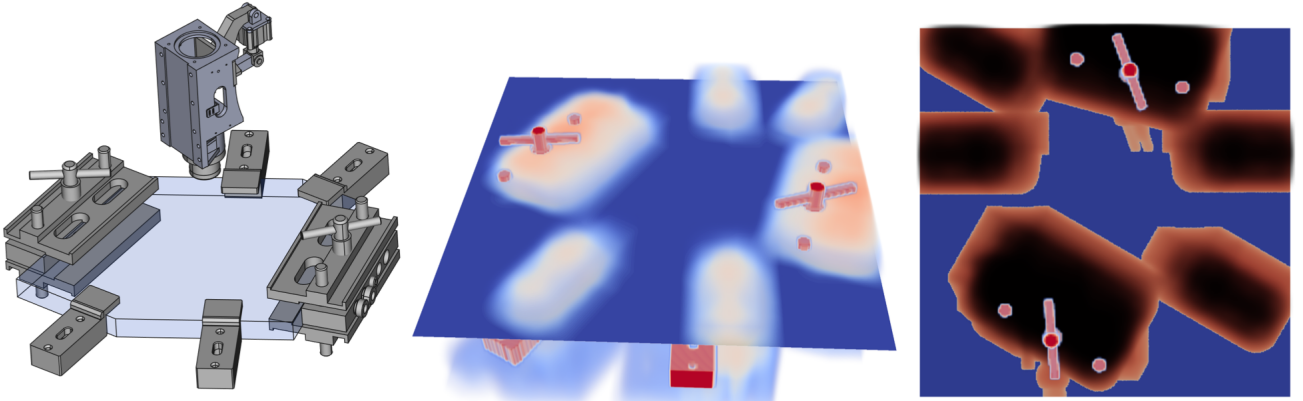


Figure 11: (a) A machining setup showing six clamps used to locate and hold a designed part, and a 2-axis instrument that can move in the plane. The envelope within which the shape must be designed is also highlighted. (b) The convolution of the reflected head with the fixtures gives a 3D field whose 2D cross-section via the plane of motion captures the collision volume at different translations. The position with zero collision volume (dark blue) are accessible. (c) The 2D cross-section of the 2.5D maximal manufacturable shape is obtained as the zero-set of the convolution field. This pointset serves as the initial design for TO (Section 5).

#### 4.4. Pruning for Accessibility with Obstacles

Consider another example in a very different setting. Suppose we are designing a part that needs to be fixtured in a crowded workholding environment so that a machining instrument is able to access specific locations without colliding with surrounding fixtures.

For simplicity, assume that the raw stock  $\Omega_0$  is a thick sheet of metal, fixtured on the machine bench as illustrated in Fig. 11 (a). The manufacturing process is an EDM wire-cut or CO<sub>2</sub> laser-cut in which the tool assembly  $T = (H \cup L)$  moves according to a planar (i.e., 2D) motion  $M \subseteq \mathbb{R}^2$  parallel to the workpiece. We assume that the translation with a vector  $(x, y) \in M$  brings the wire or laser beam, abstracted by a vertical line of zero thickness  $L$ , in contact with a line segment with  $\mathbf{x} = (x, y, z) \in \Omega_0$  for a range of  $z$ -values along the sheet thickness.

The head  $H$  cannot collide with the workpiece because they are located at different elevations, i.e.,  $(\text{sweep}(M, H) \cap \Omega) = \emptyset$  is a priori guaranteed, thus imposes no constraint. Nonetheless, the head  $H$  may collide with the fixtures  $F$ , which may extend above the workpiece, i.e.,  $(\text{sweep}(M, H) \cap F) = \emptyset$  imposes a constraint on the motion. This, in turn, imposes a constraint for manufacturability, because the motion defines the boundary of the cut shape, restricted to a curve on the 2D plane:  $M = \partial\Omega \cap \mathbb{R}^2$ . In other words, designing the as-manufactured part's shape amounts to designing the motion, because every translation of the wire or laser beam is in one-to-one correspondence with a point on the part's boundary at which there is no collision between the head and the fixtures.

**Step 1.** The moving head  $H$  may not collide with the fixtures  $F$  when swept under the motion  $M$ , i.e.,  $(\text{sweep}(M, H) \cap F) = \emptyset$ , i.e.,  $\text{sweep}(M, H) \subseteq F^c$ . This is written in the standard form  $\Gamma(\Omega) \subseteq E$ . Equivalently, for

all translations  $(x, y) \in M$  we have  $((H + (x, y, 0)) \cap F) = \emptyset$ , i.e.,  $(H + (x, y, 0)) \subseteq F^c$  which is in pointwise form  $\gamma(\mathbf{x}) \subseteq E$  for  $\mathbf{x} = (x, y, 0)$ . Notice that  $\gamma(\mathbf{x}) := (H + \mathbf{x})$  does not depend on  $\Omega$ , as required.

**Step 2.** Using the definitions in (43), we construct a PMC test for the maximal shape in the design space that satisfies this pointwise constraint:

$$\mathbf{1}_{\Omega_2^*}(x, y, z) = \begin{cases} 1 & \text{if } (H + (x, y, 0)) \subseteq F^c, \\ 0 & \text{otherwise.} \end{cases} \quad (49)$$

It is important to note that our success in defining a pointwise constraint (hence a PMC) depended on the assumption of planar translation at a higher elevation than the part, which guaranteed  $(H + (x, y, 0)) \subseteq \Omega^c$ . Otherwise, the correct constraint in (49) would have  $(F \cup \Omega)^c = (F^c \cap \Omega^c)$  instead of  $F^c$  on the right-hand side, making it stricter. But we cannot define the maximal element  $\Omega_2^*$  and its corresponding feasibility halfspace  $H_2 = \mathcal{P}^*(\Omega_2^*)$  in terms of a particular instance  $\Omega \in H_2$  (circular definition).

**Step 3.** Once again, we can leverage the dual properties of the FP- and IP-solvers to compute an explicit or implicit representation of the 2.5D maximal manufacturable solid.

The FP-solver can be any collision detection algorithm between arbitrary solids, taking as input the displaced head  $(H + (x, y, 0))$  above a particular query point  $(x, y, z) \in \Omega_0$  and the stationary fixtures  $F$ . Therefore, one can sample the design domain (i.e., the raw stock) over a 2D grid  $G$  and construct a bitmap image, representing the 2D section of the 2.5D maximal solid, by testing (49) for all  $(x, y) \in G$ . Every test requires invoking the collision detection algorithm, and can be done in parallel.

Alternatively, one can construct an IP-solver to compute the collection of all collision-free 2D translations (i.e., the

configuration space obstacle [5]). Since we are dealing with solids and regularized intersections, we can rewrite the set constraint  $(H + (x, y, 0)) \cap F = \emptyset$  in terms of measures  $\text{vol}[(H + (x, y, 0)) \cap F] = 0$  and convert it to an (in)equality constraint via (23). Hence, (49) becomes:

$$\mathbf{1}_{\Omega_2^*}(x, y, z) = \neg \text{sign} \circ \text{vol}[(H + (x, y, 0)) \cap F] \quad (50)$$

$$= \neg \text{sign} \int_{\mathbb{R}^3} \mathbf{1}_H(\mathbf{x}' - (x, y, 0)) \mathbf{1}_F(\mathbf{x}') dv[\mathbf{x}'], \quad (51)$$

noting that  $\mathbf{1}_{H+(x,y,0)}(\mathbf{x}') = \mathbf{1}_H(\mathbf{x}' - (x, y, 0))$  is the indicator function of the translated head. The integral on the right-hand side is a convolution  $(\mathbf{1}_{-H} * \mathbf{1}_F)(\mathbf{x})$ , evaluated at  $\mathbf{x} := (x, y, 0)$ , after a reflection  $\mathbf{1}_{-H}(\mathbf{x}') = \mathbf{1}_H(-\mathbf{x}')$ . The integrand is nonzero only at  $\mathbf{x}' \in \mathbb{R}^3$  where both indicator functions are nonzero, hence the integral does not vanish within the (measurable) regions of intersection. Substituting this relation into (51) yields:

$$\mathbf{1}_{\Omega_2^*}(x, y, z) = \begin{cases} 1 & \text{if } (\tilde{\mathbf{1}}_H * \mathbf{1}_F)(x, y, 0) = 0, \\ 0 & \text{otherwise.} \end{cases} \quad (52)$$

The convolution can be converted to pointwise multiplications in the frequency domain using (forward and inverse) Fourier transforms:

$$(\mathbf{1}_{-H} * \mathbf{1}_F) = \mathcal{F}^{-1}\{\mathcal{F}\{\mathbf{1}_{-H}\} \cdot \mathcal{F}\{\mathbf{1}_F\}\}, \quad (53)$$

which, in turn, can be rapidly computed as fast Fourier transforms (FFT) and accelerated on GPUs. Figure 11 illustrates the results of this computation. The convolution computes a 3D image in one shot using three FFT computations on two 3D bitmaps (voxelized  $-H$  and  $F$ ). However, we only need its 2D cross-section at  $z = 0$ , whose zero-set gives a 2D bitmap image representation of the 2.5D maximal solid  $\Omega_2^*$ .

The remaining **steps 4** and **5** are straightforward.

Note that everything in the above analysis would remain valid if we allowed the manufacturing instrument to rotate in the plane, except that we would have to change the constraint on the right-hand side of (49) to hold for at least one planar rotation  $R \in \text{SO}(2)$  of the head  $H$ :

$$\mathbf{1}_{\Omega_2^*}(\mathbf{x}) = \begin{cases} 1 & \text{if } \exists R \in \text{SO}(2) : (RH + (x, y, 0)) \subseteq F^c, \\ 0 & \text{otherwise.} \end{cases} \quad (54)$$

Accordingly, the convolution in (52) is adjusted:

$$\mathbf{1}_{\Omega_2^*}(\mathbf{x}) = \begin{cases} 1 & \text{if } \exists R \in \text{SO}(2) : (\mathbf{1}_{-RH} * \mathbf{1}_F)(x, y, 0) = 0, \\ 0 & \text{otherwise.} \end{cases} \quad (55)$$

in which the rotation can be parameterized as  $R = R(\theta)$  for  $\theta \in [0, 2\pi)$  and  $\mathbf{1}_{-RH}(\mathbf{x}') = \mathbf{1}_H(-R^{-1}\mathbf{x}')$  where  $R^{-1}(\theta) = R(-\theta)$  is an inverse rotation. To compute the PMC, one has to sample the rotation angles  $\theta \in [0, 2\pi]$  and for each trial rotation, resample the rotated head's 3D bitmap into the same grid in which the fixtures' are rasterized to compute the discrete convolution via FFT.

#### 4.5. When Pruning Fails: A More Complex Example

In more general manufacturing scenarios, a number of assumptions that enabled pointwise formulation in Section 4.4 are invalidated. For example, in a 5-axis CNC machine, one deals with 6D rigid motions  $(R, \mathbf{t}) \in \text{SE}(3)$  composed of 3D rotations  $R \in \text{SO}(3)$  and 3D translations  $\mathbf{t} \in \mathbb{R}^3$ . The tool assembly  $T = (H \cup C)$  is no longer guaranteed to avoid collisions with the workpiece, leading to global constraints that depend on the part's shape as well as the head, cutter, and fixtures. The configuration space obstacle  $M_\Omega := \text{obs}(O_\Omega, T)$  where  $O_\Omega = (\Omega \cup F)$  is stated as a group convolution  $\star$  operation [65], which, in turn, can be computed as a Euclidean convolution  $*$  as before:

$$\mathbf{1}_{M_\Omega}(R, \mathbf{t}) = \text{sign} \circ (\mathbf{1}_{O_\Omega} \star \mathbf{1}_{-T})(R, \mathbf{t}) \quad (56)$$

$$= \text{sign} \circ (\mathbf{1}_{O_\Omega} * \mathbf{1}_{-RT})(\mathbf{t}), \quad (57)$$

Attempting to write a PMC similar to (55) fails for several reasons; let us give it a try:

$$\mathbf{1}_{\Omega_3^*}(\mathbf{x}) \stackrel{?}{=} \begin{cases} 1 & \text{if } \exists R \in \text{SO}(3) : (\mathbf{1}_{O_\Omega} * \mathbf{1}_{-RT})(\mathbf{t}) = 0, \\ 0 & \text{otherwise.} \end{cases} \quad (58)$$

The first obvious problem is the dependency of the right-hand side on  $\Omega$ , which makes for a circular definition. Moreover, the cutter's shape cannot be ignored (unlike the case with wire-/laser-cut). Hence, there is no obvious way to assign a correspondence between the translations  $\mathbf{t} \in \mathbb{R}^3$  and the points  $\mathbf{x} \in \Omega_0$  within the design domain, unless we consider all possible contact configurations and treat boundary points differently from interior points. Last but not least, passing a collision check at the contact configuration is not sufficient for accessibility, because there may not exist a connected path from the initial configuration of the tool assembly to the cutting pose of interest. For example, if a downstream TO creates cavities in the design in 3D, none of the will be accessible (unlike 2.5D).

In the next section, we deal with constraints that cannot be stated in pointwise form due to global dependencies. We assume that the design has been pruned (using methods of this section) for all pointwise constraints to produce an initial design  $\Omega_P^* = (\Omega_1^* \cap \Omega_2^* \cap \dots \cap \Omega_{n_P}^*) \subseteq \Omega_0$  for design space exploration with regard to the remaining  $(n - n_P) = (n_G + n_L)$  global and/or local constraints.

## 5. Design Space Exploration

In this section, we present a methodology to solve the **phase 2** problem formulated in (36) of Section 3.4. Our goal is not to propose new optimization algorithms besides the many existing ones (reviewed in Section 2). Rather, we propose a general strategy to deal with constraints that *cannot* be stated in a pointwise fashion, to guide gradient-descent optimization.

In Section 5.1, we formulate multi-objective and multi-constraint optimization. We extend existing approaches



to deal with heterogeneous constraints, including not only physics-based constraints obtained from FEA but also kinematics-based constraints obtained from accessibility analysis for machining.

In order to move *deterministically* in the design space in directions that consistently reduce the violation of these constraints, we quantify their sensitivities to hypothetical local changes in the design. Different gradient-like quantities can be defined for different design representations. In Section 5.3, we demonstrate our approach specifically for defining, augmenting, and filtering topological sensitivity fields (TSF) [78] with global and local constraints.

### 5.1. Multi-Objective and Multi-Constraint Optimization

Fixed-point iteration (a.k.a. Picard iteration) [79] is an effective approach for numerically solving multi-objective optimization problems, where the problem is iteratively solved through series of outer- and inner-loops. As the value of each objective function is changed in the outer-loop, its value is kept fixed in the inner loop. The fixed objective functions are treated as equality constraints for the single-objective inner-loop optimization. Among the many popular approaches, we use a Pareto tracing levelset TO approach (PareTO) [20], because it produces valid designs (i.e., solids) at all intermediate steps. It was shown in [72] that Pareto tracing can also be extended to density-based approaches such as solid isotropic material with penalization (SIMP) [1].

For example, in classical TO, the goal is to obtain light-weight stiff structures, leading to two competing objectives (mass and compliance) with a one-dimensional Pareto frontier, illustrated for different examples in Figs. 4, 14, and 13 (a). The problem can be formulated as follows:

$$\text{Find } \Omega \in \mathcal{D}_P^* : \begin{cases} \text{minimize } \bar{V}_\Omega \text{ and } J_\Omega = [\mathbf{f}]^T[\mathbf{u}_\Omega], \\ \text{subject to } [K_\Omega][\mathbf{u}_\Omega] = [\mathbf{f}], \end{cases} \quad (59)$$

where the volume fraction  $\bar{V}_\Omega := \text{vol}[\Omega]/\text{vol}[\Omega_P^*]$  is the ratio of the (unknown)  $\text{vol}[\Omega]$  to the initial design's volume  $\text{vol}[\Omega_P^*]$ , where  $\Omega_P^* \subseteq \Omega_0$  is the maximal feasible pointset obtained from pruning in Section 4. Classical TO in the absence of pruning is subsumed as a special case when  $\Omega_P^* = \Omega_0$ . The second objective function  $J_\Omega = [\mathbf{f}]^T[\mathbf{u}_\Omega]$  is the compliance (i.e., strain energy) obtained from FEA, in which  $[\mathbf{u}_\Omega]$  is the discretized displacement field and  $[\mathbf{f}]$  is the external load vector given as (Neumann) boundary conditions. The FEA also appears as an equality constraint  $[K_\Omega][\mathbf{u}_\Omega] = [\mathbf{f}]$  in which  $[K_\Omega]$  is the stiffness matrix obtained from the design shape, material properties, and restraints given as (Dirichlet) boundary conditions.

We can reformulate the problem as a single-objective optimization for a fixed volume fraction:

$$\text{Find } \Omega \in \mathcal{D}_P^* : \begin{cases} \text{select target } \bar{V}_\Omega^{\text{targ}} \in (0, 1], \\ \text{ILL: } \begin{cases} \text{minimize } J_\Omega = [\mathbf{f}]^T[\mathbf{u}_\Omega], \\ \text{s.t. } \bar{V}_\Omega = \bar{V}_\Omega^{\text{targ}}, \\ \text{s.t. } [K_\Omega][\mathbf{u}_\Omega] = [\mathbf{f}], \end{cases} \end{cases} \quad (60)$$

where ILL stands for inner-loop iteration. Within each ILL, a single-objective optimization is solved to minimize compliance  $J_\Omega$  subject to a fixed volume fraction constraint  $\bar{V}_\Omega = \bar{V}_\Omega^{\text{targ}}$  for a fixed  $0 < \bar{V}_\Omega^{\text{targ}} \leq 1$ . In PareTO [20], one starts off on the Pareto frontier at the right-most extreme with  $\Omega := \Omega_P^*$  and  $\bar{V}_\Omega^{\text{targ}} = 1$ , i.e., the best-case scenario for compliance at the cost of the largest volume. The algorithm incrementally removes material to decrease  $\bar{V}_\Omega^{\text{targ}}$  by introducing holes in the design, without deviating too much from the Pareto front. The ILL is a fixed-point iteration that applies local modifications to the new design to bring it back to the Pareto front, as shown schematically in Fig. 13 (a). See [18, 20, 80, 81] for more details on PareTO and its various applications.

The inner-loop optimization can be expressed as local minimization of the Lagrangian defined as:

$$\mathcal{L}_\Omega := [\mathbf{f}]^T[\mathbf{u}_\Omega] + \lambda_1(\bar{V}_\Omega - \bar{V}_\Omega^{\text{targ}}) + [\lambda_2]^T \left( [K_\Omega][\mathbf{u}_\Omega] - [\mathbf{f}] \right). \quad (61)$$

The Karush–Kuhn–Tucker (KKT) conditions [46] for this problem are given by  $\nabla \mathcal{L}_\Omega = 0$  in which the gradient is defined by partial differentiation with respect to the independent variables; namely, the design variables used to represent  $\Omega$  and the Lagrange multipliers  $\lambda_1$  and  $[\lambda_2]$ . The latter simply encodes the constraints into  $\nabla \mathcal{L}_\Omega = 0$ :

$$\frac{\partial}{\partial \lambda_1} \mathcal{L}_\Omega = (\bar{V}_\Omega - \bar{V}_\Omega^{\text{targ}}) := 0, \quad (62)$$

$$\frac{\partial}{\partial \lambda_2} \mathcal{L}_\Omega = [K_\Omega][\mathbf{u}_\Omega] - [\mathbf{f}] := [0], \quad (63)$$

On the other hand, differentiation with respect to  $\Omega \in \mathcal{D}_P^*$  depends on the particular parameterization used to represent the design by a finite set of decision variables for optimization. These variables can be geometric/size variables (e.g., thickness in truss optimization), density variables (e.g., volume fractions in SIMP), and so on. Our goal is to present a representation-agnostic form in terms of TSF.

If we use a prime symbol  $(\cdot)'$  to represent the generic (linear) differentiation of a function with respect to  $\Omega$ , we obtain (via chain rule):

$$\begin{aligned} \mathcal{L}'_\Omega &= [\mathbf{f}]^T[\mathbf{u}'_\Omega] + \lambda_1 \bar{V}'_\Omega + [\lambda_2]^T \left( [K_\Omega][\mathbf{u}_\Omega] \right)', \\ &= \left( [\mathbf{f}]^T + [\lambda_2]^T [K_\Omega] \right) [\mathbf{u}'_\Omega] + \lambda_1 \bar{V}'_\Omega + [\lambda_2]^T [K'_\Omega][\mathbf{u}_\Omega], \end{aligned} \quad (64)$$

Computing  $[\mathbf{u}'_\Omega]$  is prohibitive, as it requires calling FEA as many times as the number of independent variables used to represent  $\Omega$ . The common solution is to choose  $[\lambda_2]$  such that  $[\mathbf{f}]^T + [\lambda_2]^T [K_\Omega] = [0]$  (adjoint problem) [46]:

$$\mathcal{L}'_\Omega = \lambda_1 \bar{V}'_\Omega + [\lambda_2]^T [K'_\Omega][\mathbf{u}_\Omega], \text{ if } [\lambda_2] := -[K_\Omega]^{-1}[\mathbf{f}], \quad (65)$$

In general, if we have  $n_O > 0$  global objective functions and another  $n_G \geq 0$  global (in)equality constraints, (64) can be generalized as:

$$\mathcal{L}'_\Omega := \sum_{n_C < i \leq n_C + n_O} \bar{\lambda}_i f'_i(\Omega) + \sum_{n_P < i \leq n_P + n_G} \bar{\lambda}_i g'_i(\Omega), \quad (66)$$

in which the indexing scheme is to reconcile with that of Section 3.4. We can simplify the notation by introducing  $F_j(\Omega) := f_{n_C+j}(\Omega) - f_{n_C+j}^{\text{targ}}$  for  $0 < j \leq n_O$  and  $F_j(\Omega) := g_{n_P-n_O+j}(\Omega)$  for  $n_O < j \leq n_O + n_G$ , hence:

$$\mathcal{L}'_{\Omega} = \sum_{0 < j \leq n_O + n_G} \lambda_j F'_j(\Omega), \quad (67)$$

## 5.2. Coupling Physical and Manufacturing Constraints

The ILI in (60) can be generalized to accommodate other global objective functions and global constraints. For example, suppose the part is to be 3D printed at a given build direction. An additional global (in)equality constraint is imposed in terms of an upper-bound  $\bar{V}_{UB} \geq 0$  on the total volume of support material that is needed based on an overhang angle criterion [18]:

$$\text{Find } \Omega \in D_P^* : \begin{cases} \text{select target } \bar{V}_{\Omega}^{\text{targ}} \in (0, 1], \\ \text{ILLI: } \begin{cases} \text{minimize } J_{\Omega} = [\mathbf{f}]^T[\mathbf{u}_{\Omega}], \\ \text{s.t. } \bar{V}_{\Omega} = \bar{V}_{\Omega}^{\text{targ}}, \\ \text{s.t. } [K_{\Omega}][\mathbf{u}_{\Omega}] = [\mathbf{f}], \\ \text{s.t. } \bar{V}_{S_{\Omega}} \leq \bar{V}_{UB}, \end{cases} \end{cases} \quad (68)$$

where  $S_{\Omega} \subseteq \Omega^c$  represents the support structure. Its volume fraction  $\bar{V}_{S_{\Omega}} = \text{vol}[S_{\Omega}]/\text{vol}[\Omega_P^*]$  can be computed as a function of the angle between surface normals and the build direction at every outer-loop iteration [18]. The Lagrangian in (61) is further augmented by adding another term  $\lambda_3(\bar{V}_{S_{\Omega}} - \bar{V}_{UB})$  and the generic sensitivity in (65) is updated by incorporating  $\bar{V}'_{S_{\Omega}}$  as:

$$\mathcal{L}'_{\Omega} = \lambda_1 \bar{V}'_{\Omega} + [\lambda_2]^T [K'_{\Omega}][\mathbf{u}_{\Omega}] + \lambda_3 \bar{V}'_{S_{\Omega}}. \quad (69)$$

Figure 12 compares the solution to a TO problem with and without constraining the support material volume (adopted from [18]). Observe that optimization without the support constraint exits the feasibility halfspace with respect to this constraint for design volume fractions less than 70%. For lighter designs, the removed design material comes at the expense of additional support material, hence costlier manufacturing. The fully constrained optimization with augmented sensitivity as in (69) dramatically increases the number of feasible and Pareto-optimal options, even at volume fractions lower than 70%.

Another example is TO subject to accessibility constraints for machining. Once again, we can impose a global (in)equality constraint in (7) to in terms of an upper-bound  $\bar{V}_{UB} \geq 0$  on the total inaccessible volume:

$$\text{Find } \Omega \in D_P^* : \begin{cases} \text{select target } \bar{V}_{\Omega}^{\text{targ}} \in (0, 1], \\ \text{ILLI: } \begin{cases} \text{minimize } J_{\Omega} = [\mathbf{f}]^T[\mathbf{u}_{\Omega}], \\ \text{s.t. } \bar{V}_{\Omega} = \bar{V}_{\Omega}^{\text{targ}}, \\ \text{s.t. } [K_{\Omega}][\mathbf{u}_{\Omega}] = [\mathbf{f}], \\ \text{s.t. } 1 - \bar{V}_{R_{\Omega}} - \bar{V}_{\Omega} \leq \bar{V}_{UB}, \end{cases} \end{cases} \quad (70)$$

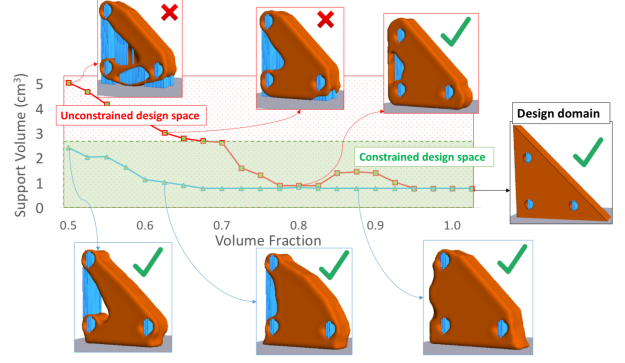


Figure 12: TO with and without augmenting the sensitivity with constraints on the support material needed for 3D printing along the vertical build direction [18]. Many of the solutions without considering the support constraint will still satisfy that constraint due to the larger volume fraction occupied by the design itself. However, as the material is reduced from the design below 70%, the TO generates designs that require more support material.

where  $R_{\Omega} \subseteq \Omega^c$  represents the maximal accessible region outside the design for a combination of tools and approach directions in 3-axis milling [7]. The volume fraction of the inaccessible regions is  $1 - \bar{V}_{R_{\Omega}} - \bar{V}_{\Omega}$  where  $\bar{V}_{R_{\Omega}} = \text{vol}[R_{\Omega}]/\text{vol}[\Omega_P^*]$  and  $\bar{V}_{\Omega} = \text{vol}[\Omega]/\text{vol}[\Omega_P^*]$ , as before. The Lagrangian in (61) is further augmented by adding another term  $\lambda_3(1 - \bar{V}_{R_{\Omega}} - \bar{V}_{\Omega} - \bar{V}_{UB})$ , hence:

$$\mathcal{L}'_{\Omega} = \lambda_1 \bar{V}'_{\Omega} + [\lambda_2]^T [K'_{\Omega}][\mathbf{u}_{\Omega}] + \lambda_3 (\bar{V}'_{R_{\Omega}} - \bar{V}'_{\Omega}) \quad (71)$$

$$= (\lambda_1 - \lambda_3) \bar{V}'_{\Omega} + [\lambda_2]^T [K'_{\Omega}][\mathbf{u}_{\Omega}] + \lambda_3 \bar{V}'_{R_{\Omega}}. \quad (72)$$

One can alternatively formulate the optimization problem for accessibility using the local constraint in (14):

$$\text{Find } \Omega \subseteq \Omega_P^* \text{ to } \begin{cases} \text{select target } \bar{V}_{\Omega}^{\text{targ}} \in (0, 1], \\ \text{ILLI: } \begin{cases} \text{minimize } J_{\Omega} = [\mathbf{f}]^T[\mathbf{u}_{\Omega}], \\ \text{s.t. } \bar{V}_{\Omega} = \bar{V}_{\Omega}^{\text{targ}}, \\ \text{s.t. } [K_{\Omega}][\mathbf{u}_{\Omega}] = [\mathbf{f}], \\ \text{s.t. } [\mathbf{1}_{\Omega} * \mathbf{1}_{-T}] = [0], \end{cases} \end{cases} \quad (73)$$

in which the inaccessibility measure  $\mu_{\Omega}(\mathbf{x}) = (\mathbf{1}_{O_{\Omega}} * \tilde{\mathbf{1}}_T)$  in (14), defined as the convolution in (15) is discretized to  $[\mu_{\Omega}] = [\mathbf{1}_{O_{\Omega}} * \tilde{\mathbf{1}}_T]$  and further simplified to  $[\mu_{\Omega}] = [\mathbf{1}_{\Omega} * \tilde{\mathbf{1}}_T]$  assuming that the stationary obstacle  $O_{\Omega} = (\Omega \cup F)$  includes only the target design  $O_{\Omega} = \Omega$ , ignoring the fixtures  $F := \emptyset$ . The tool assembly  $T = (HUC)$  includes the holder  $H$  and cutter  $C$ , as before. We use a conservative measure, aiming for no allowance for inaccessibility (i.e.,  $\mu_0 := 0$  in (14)) hence  $[\mathbf{1}_{\Omega} * \tilde{\mathbf{1}}_T] = [0]$  over all discrete elements (e.g., voxels) wherever possible in the design domain. The discrete convolution is computed using two forward FFTs on  $[\mathbf{1}_{\Omega}]$  and  $[\tilde{\mathbf{1}}_T]$ , a pointwise multiplication of their frequency domain grids, and an inverse FFT to obtain  $[\mathbf{1}_{\Omega} * \tilde{\mathbf{1}}_T]$  in the physical domain (as a voxelized field).

Hereon, we assume that reducing the volume is always an objective/cost function, hence the outer-loop is always

set up to incrementally decrease the volume fraction budget  $\bar{V}_\Omega^{\text{targ}} \in (0, 1]$  starting from the initial value  $\bar{V}_\Omega^{\text{targ}} := 1$  on the costlier extreme of the Pareto front. The optimization problem is formulated in general as:

$$\text{Find } \Omega \in \mathcal{D}_\mathbb{P}^* : \begin{cases} \text{select target } \bar{V}_\Omega \in (0, 1], \\ \text{LLI: } \begin{cases} \text{minimize } f_i(\Omega), \quad n_C < i \leq n_C + n_O, \\ \text{s.t. } \bar{V}_\Omega = \bar{V}_\Omega^{\text{targ}}, \\ \text{s.t. } g_i(\Omega) \leq 0, \quad n_P < i \leq n_P + n_G, \\ \text{s.t. } g_i(\mathbf{x}; \Omega) \leq 0, \quad n_P + n_G < i \leq n_C, \end{cases} \end{cases} \quad (74)$$

### 5.3. Sensitivity Fields for Global & Local Constraints

In this section, we use TSF to define  $\mathcal{L}'_\Omega$  and  $F'_i(\Omega)$  in (67) in a representation-independent form. Let us first look at a few examples with manufacturability constraints in addition to the physical constraints in (60).

The notion of a TSF is widely applied in the TO literature [20, 78] as a means to guide the optimization process in moving from one candidate solution to another in the search for local optima. Intuitively, the TSF is a gradient-like operator for pointsets that quantifies *the global effect of local changes* of a given function (e.g., violation of a global constraint). We couple the TSFs for various global and local constraints in three distinct steps:

- *Defining TSFs for Global Constraints:* For global constraints of the general form  $g_i(\Omega) \leq 0$ , we define one TSF per constraint to measure how its violation changes after removing a hypothetical small neighborhood (called an “inclusion”) at a given point.
- *Augmenting TSFs for Global Constraints:* The individual TSFs are linearly combined for all global constraints (including the fixed objective functions).
- *Penalizing TSFs via Local Constraints:* For local constraints of the general form  $g_i(\mathbf{x}; \Omega) \leq 0$ , we penalize the TSF of the global constraints by a linear combination of the violation of local constraints.

We elaborate in Sections 5.3.1 through 5.3.3.

#### 5.3.1. Defining Sensitivities for Global Constraints

For every function  $F_i : \mathcal{D}_\mathbb{P}^* \rightarrow \mathbb{R}$  that depends globally on the design (objective function or constraint), we define a field  $\mathcal{T}_i : (\Omega_\mathbb{P}^* \times \mathcal{D}_\mathbb{P}^*) \rightarrow \mathbb{R}$  as its TSF via:

$$\mathcal{T}_i(\mathbf{x}; \Omega) := \lim_{\epsilon \rightarrow 0^+} \frac{F_i(\Omega - B_\epsilon(\mathbf{x})) - F_i(\Omega)}{\text{vol}[\Omega \cap B_\epsilon(\mathbf{x})]}, \quad (75)$$

for  $0 < i \leq n_O + n_C$ .  $B_\epsilon(\mathbf{x}) \subset \Omega_0$  is a small 3D ball of radius  $\epsilon \rightarrow 0^+$  centered at a given query point  $\mathbf{x} \in \Omega$ . The numerator of the limit evaluates the (presumably infinitesimal) change in  $F_i(\Omega)$  when the candidate design is modified as  $\Omega \mapsto (\Omega - B_\epsilon(\mathbf{x}))$ , i.e., by puncturing an infinitesimal cavity at the query point. The denominator

$\text{vol}[\Omega \cap B_\epsilon(\mathbf{x})] = O(\epsilon^3)$  as  $\epsilon \rightarrow 0^+$  measures the volume of the cavity. For internal points  $\mathbf{x} \in i\Omega$  (i.e., points that are not exactly on the topological boundary) one has  $\text{vol}[\Omega \cap B_\epsilon(\mathbf{x})] = \text{vol}[B_\epsilon(\mathbf{x})]$  as  $\epsilon \rightarrow 0^+$ .

#### 5.3.2. Combining Sensitivities for Global Constraints

It was shown in [82] that the method of augmented Lagrangian can be extended to TSFs, and its effectiveness was demonstrated by TO of multi-load structures under deformation and stress constraints. We apply the linear combination of the generic form in (67) to compute an “augmented” TSF to couple the global (in)equality constraints:

$$\mathcal{T}(\mathbf{x}; \Omega) := \sum_{0 < j \leq n_O + n_G} \lambda_j \mathcal{T}_j(\mathbf{x}; \Omega). \quad (76)$$

Note that the above sum provides a representation-independent mathematical definition for the gradient in (67) with respect to the (unparameterized) pointset  $\Omega \in \Omega_\mathbb{P}^*$ . Rather than quantifying a direction of steepest descent for moving in a particular parameter space,  $\mathcal{T}(\mathbf{x}; \Omega)$  identifies the set of points  $\mathbf{x} \in \Omega$  that are *contributing the most to the violation of constraints*. A proper direction to move in the (unparameterized) design space  $\mathcal{D}_\mathbb{P}^*$  is to remove the points with maximal TSF.

The coefficients  $\lambda_j > 0$  have to be either computed by solving adjoint problems – as we showed for the case of strain energy in (65)—or selected using *adaptive weighting* schemes that are mainstream in multi-objective and multi-constraint TO [82, 83].

#### 5.3.3. Penalizing Sensitivities via Local Constraints

The TSF operator maps global constraints to fields that vary depending on  $\mathbf{x} \in \Omega$ . The local constraints are already defined as fields that vary in a similar fashion (i.e., are of the same “type” as the TSF). Hence, we can penalize the TSF in (76) with local constraints as:

$$\hat{\mathcal{T}}(\mathbf{x}; \Omega) := \mathcal{T}(\mathbf{x}; \Omega) + \sum_{n_P + n_G < i \leq n_C} \kappa_i g_i(\mathbf{x}; \Omega). \quad (77)$$

The choice of coefficients  $\kappa_i > 0$  might need experimenting with the TO to adjust the relative importance of different constraints and improve convergence properties.

#### 5.4. Pareto Front Tracing by Fixed-Point Iterations

The TSF orders the points in the design domain according to the potential impact of removing their local neighborhoods on objective function and constraints. An incremental improvement to the design is one that eliminates the points with the lowest TSF (e.g., the bottom 5%). We define an ‘ $\tau$ -modified’ (potentially infeasible) design  $\Omega(\tau) \subset \Omega$  by a PMC in terms of the current design  $\Omega$ :

$$\mathbf{1}_{\Omega(\tau)}(\mathbf{x}) := \begin{cases} 1 & \text{if } \hat{\mathcal{T}}(\mathbf{x}; \Omega) \geq \tau, \\ 0 & \text{otherwise,} \end{cases} \quad (78)$$

$$\text{i.e., } \Omega(\tau) := \{\mathbf{x} \in \Omega \mid \hat{\mathcal{T}}(\mathbf{x}; \Omega) \geq \tau\}. \quad (79)$$

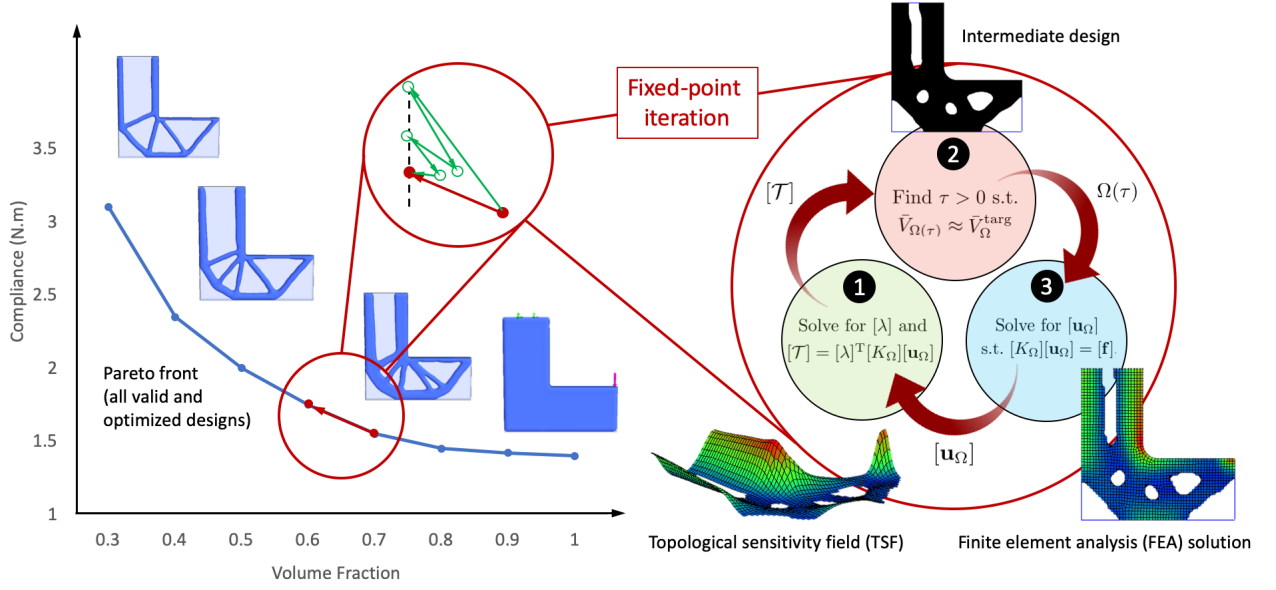


Figure 13: Using fixed-point iteration, the design is iteratively modified for every small reduction in the volume such that the optimality conditions and performance constraints remain satisfied at every point along the Pareto front.

where the isolevel threshold  $\tau > 0$  determines a step size for incremental change, e.g.,  $\tau := 0.05$  means we are removing the least sensitive 5%. It is important to select a small value so that only a small subset with  $\hat{\mathcal{T}}(\mathbf{x}; \Omega) \geq \tau$  is removed to obtain a shape that is not too different. The new design marginally violates the constraints and slightly deviates from the Pareto front (Fig. 13 (a)). However, it is close enough to the front that it can be brought back by a fixed-point iteration (Fig. 13 (b, c)). The iteration may not converge if the step size is too large. But if it does, it produces another feasible and (locally) Pareto-dominant design that is slightly lighter.

**Optimization Loops.** Here is a general algorithm:

1. Pick a value  $\delta > 0$  for the desired change in volume fraction for the outer-loop iteration.
2. Compute  $\hat{\mathcal{T}}(\mathbf{x}; \Omega)$  from (76) and (77) and normalize it with its maximum value over the current design.
3. Initialize  $\Omega(\tau) \subseteq \Omega$  using (79) with a reasonably small initial  $\tau \leftarrow \tau_0$  to start the fixed-point iteration:
  - (a) Cycle over the FP-solvers and update the performance fields  $\mathcal{A}_i(\Omega) \rightarrow \mathcal{A}_i(\Omega(\tau))$  (e.g., the constrained physical or kinematic properties) for the  $\tau$ -modified design obtained from (78).
  - (b) Re-evaluate the constraints using the updated performance results; recompute the TSF using (76) and (77) everywhere accordingly.
  - (c) Find  $\tau > 0$  such that the  $\tau$ -modified design in (79) with the updated TSF has the desired reduction in volume fraction, i.e.,  $\bar{V}_{\Omega(\tau)} \approx (\bar{V}_{\Omega} - \delta)$ .

- (d) Repeat (a–c) until the  $\tau$ -modified design does not change. The result is feasible with respect to the constraints and is Pareto-dominant.

4. Repeat (1–3) until the volume fraction reaches the smallest feasible value to sustain the requirements.

**Procedure.** Here is a systematic procedure to *explore* the pruned design space, i.e., trace a locally Pareto-optimal family of alternative design variants  $D_{\text{dom}}^* \subset D_{\text{P}}^*$  by recurrent incremental thresholding of (augmented and penalized) TSF, defined in terms of global and local constraints:

- **Step 0.** Start at the extreme end of the Pareto front (maximal volume) by initializing the design with the maximal pointset obtained from pruning  $\Omega \leftarrow \Omega_{\text{P}}^*$ .
- **Step 1.** Express the global objective functions and global and local constraints for a given design  $\Omega \in D_{\text{P}}^*$  to formulate the problem in the general form of (74).
- **Step 2.** Define a subroutine to evaluate TSFs for each global objective function and global constraint using (75), combine them using (76), and penalize them with local constraints using (77).
- **Step 3.** Invoke the outer-loop optimization algorithm explained above to incrementally reduce the material by thresholding the TSF.
- **Step 4.** Within the inner-loop (fixed point iteration) cycle over FP-solvers to evaluate the objective functions and constraint upon every incremental change in the outer-loop. Repeat until the deviated solution converges back on the Pareto front.

- Repeat **steps 2–4** sequentially until the algorithm cannot find a solution for after removing enough material, i.e., arrives at other extreme end of the Pareto front (minimal volume).

### 5.5. Exploration after Uncoupled Assembly Constraints

Let us consider the (secondary) car hood latch problem adopted from [14] and presented in Section 1 with the following kinematic and physical constraints:

1. The latch must retain special features designated by the designer, as illustrated in Fig. 14.
  - One feature ensures that its mating pin (moving vertically up and down) rotates the latch by  $21^\circ$  due to sliding contact maintained through a spring (not shown here).
  - The other feature is for safety considerations; it ensures that if the pin moves upwards in a sudden reverse motion – due to a failure of the primary latch – the secondary latch stops clap it to prevent the car hood from opening.
2. As the latch rotates around its pivot from  $0^\circ$  to  $21^\circ$ , it must remain completely within a safe region of space to avoid interference with other car parts.
3. The latch is to be manufactured from stainless steel 304 using a metal AM process.
4. The latch should not weigh more than 0.30 pound.
5. The latch will experience loads at pre-determined points/surfaces, including the contact forces with the pin exerted by the spring. Under these loads, its maximum deflection must not exceed 0.03 inches.

Such a diverse set of requirements is quite common, and should be simultaneously handled by the computational design framework. We note from the first requirement that modeling design intent and synthesizing functional features to satisfy them are difficult without knowing substantial information about the application. These features are given in a pre-processing step (Fig. 14). Nevertheless, a substantial remaining portion of the geometry is not defined by functional features and can be optimized. The remaining requirements are systematically solved using the methods presented in this paper.

**Step 0.** Recall from Section 4.3 that requirement 2 can be satisfied upfront (without premature optimization) by pruning the design space via an IP-solver. We start the TO with the initial design  $\Omega_1^* := \text{unsweep}(M, E)$  where  $M = \{R(\theta) \in \text{SO}(2) \mid 0 \leq \theta \leq 21^\circ\}$  is the collection of all rotations that the latch can go experience, and  $E \subseteq \mathbb{R}^3$  is the containment envelope (Fig. 15).

Since TO is a material-reducing procedure, the remaining requirements 3–5 can be satisfied by TO without violating the containment constraint.

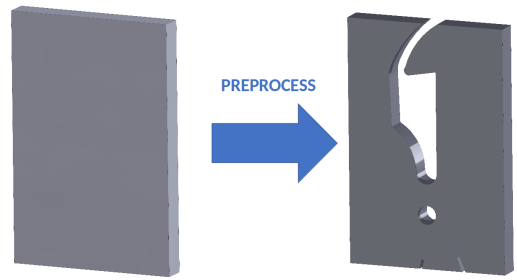


Figure 14: Functional surfaces are specified in pre-processing.

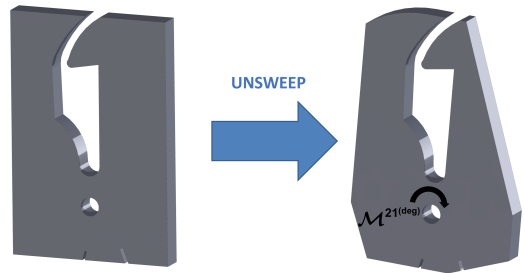


Figure 15: The **Un sweep** removes parts of the pre-processed initial design that would exit the envelope for any clockwise rotation of  $\theta \in [0^\circ, 21^\circ]$  around the pivot.

**Steps 1, 2.** In the absence of manufacturing constraints, the physics-based constraints for this problem are posed in common form of (59). The upper-bound on the weight can be converted to an upper-bound on volume fraction  $\bar{V}_\Omega \leq \bar{V}_\Omega^{\text{targ}}$  where  $\bar{V}_\Omega^{\text{targ}} = (0.30 \text{ lb}/\rho_{\text{SS304}})/\text{vol}[\Omega_1^*]$  using the known density of SS304.

The upper-bound on deflection  $\delta_\Omega(\mathbf{x}) \leq \delta_{\text{UB}} := 0.03''$  need not be stated as a separate constraint, because it implies an upper-bound on compliance, hence a lower-bound on the volume fraction.

**Steps 3, 4.** At every outer-loop iteration, the maximal deflection increases due to removed material. The algorithm checks if the deflection constraint is violated and stops at the lightest possible solution.

Within the inner-loop fixed point iteration, the TSF is computed as in (65), based on which the  $\tau$ -modified design  $\Omega(\tau)$  is extracted as the  $\tau$ -superlevel set of the TSF. Subsequently, the FEA solver is invoked to solve  $[K_{\Omega(\tau)}][\mathbf{u}_{\Omega(\tau)}] = [\mathbf{f}]$ . Based on the updated stiffness matrix  $[K_{\Omega(\tau)}]$  and displacement field  $[\mathbf{u}_{\Omega(\tau)}]$  in response to the boundary conditions, the Lagrange multipliers are updated via (65) as  $[\lambda_2] = -[K_{\Omega(\tau)}]^{-1}[\mathbf{f}]$  and the TSF in (76) is recomputed. The iteration is repeated until the design remains unchanged.

Figure 16 illustrates the Pareto front for solving the above problem, starting from the pruned design domain  $\Omega_p^*$  as prescribed above (strategy 1). The results are compared against the case when the algorithm starts from the initial design domain  $\Omega_0$  (strategy 2), ignoring the contain-

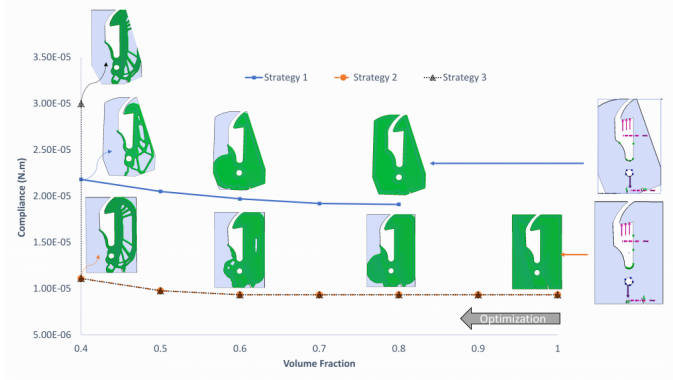


Figure 16: Optimization fronts traced by different strategies. The first strategy that applies TO to the pruned feasible design subspace of the containment constraint is the most computationally rational, as the entire family of solutions satisfy all requirements.

ment constraint (requirement 2). The latter is an example of premature optimization, after which there is no guarantee that the design can be fixed to take the containment constraint into account. The graph also shows an incorrect attempt to fix the design as in Fig. 2 of Section 1, leading to an infeasible and suboptimal design (strategy 3).

### 5.6. Exploration after Uncoupled Accessibility Constraints

Let us next consider the problem of design for manufacturability in Section 4.4 with the setup shown earlier in Fig. 11. Once again, functional features are specified in pre-processing,<sup>9</sup> as illustrated in Fig. 17. The boundary conditions are shown on the top-right corner of Fig. 18, including both forces and restrained surfaces. The underlying material is stainless steel with Young’s modulus  $Y = 200$  GPa and Poisson’s ratio  $\nu = 0.33$ .

**Step 0.** We showed in Section 4.4 that the design space can be pruned with respect to the accessibility of a 2-axis CNC instrument, where the 2D cross-section of the 2.5D maximal pointset was obtained as the 0-level set of a 3D convolution field between the head  $H$  and fixtures  $F$  (both in 3D), i.e.,  $\Omega_2^* \cong (\mathbf{1}_{-H} * \mathbf{1}_F)^{-1}(0)$ .

**Steps 1, 2.** We are interested in finding a set of designs with maximal stiffness while reducing the volume of the pruned design domain by another 60%.

All the optimized designs must have uniform cross-sections along wire-/laser-cutting direction (i.e., are 2.5D). This constraint can be imposed either by applying a 2D TO to the cross-section of the initial design and extruding its results, or by using a 3D TO with a through-cut filtering of the TSF shown in Fig. 5 (c) of Section 1. We use the latter (PareTO in 3D) for this example.

<sup>9</sup>We are assuming that these features are also accessible. Otherwise, they could be introduced upfront in the raw stock and be modified by designer through trial and error.

The remaining **steps 3** and **4** are similar to the previous example. The only FP-solver in the loop is a standard FEA, in absence of coupled manufacturing constraints, noting that manufacturability is a priori guaranteed in the pruning phase. In the next example, we consider a problem in which the manufacturing constraints cannot be pruned and has to be coupled with the physical constraints within the inner-loop fixed-point iteration.

Figure 19 shows the fixturing setup, raw stock, maximal manufacturable domain (i.e., initial design for TO), and the optimized design at 40% volume fraction. Figure 18 shows the Pareto front as it is traced from 100% to 40% volume fraction. As with the previous example, the material reducing nature of TO ensures that it does not violate the manufacturability constraint satisfied in Section 4.4.

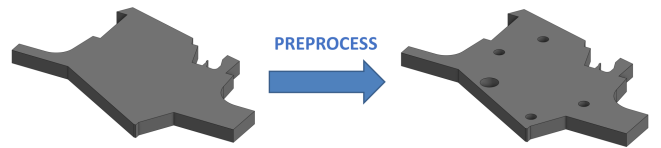


Figure 17: Functional surfaces are specified in pre-processing.

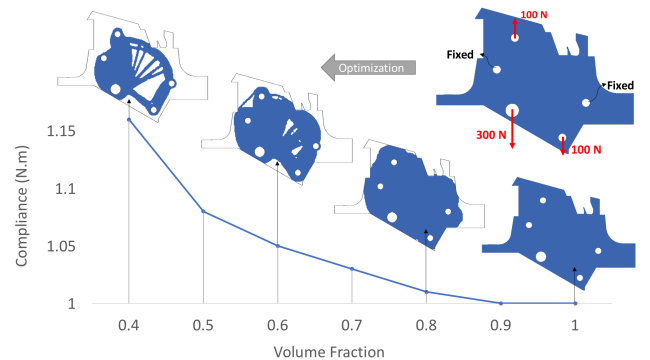


Figure 18: Pareto front of accessible designs optimized under illustrated loading conditions. The lightest optimized design at 40% volume fraction is also shown in Fig. 19.

### 5.7. Exploration with Coupled Accessibility Constraints

The accessibility constraint of Section 5.6 was solely dependent on the surrounding fixtures, which enabled us to enforce it by pruning the design space before TO. We argued in Section 4.5 that this is not possible for general accessibility problems in which the design’s (unknown) shape affects the evaluation of the constraint. In this section we focus on accessibility constraints that evolve throughout the design space exploration via TO. They are coupled with physical constraints (evaluated by FEA).

In Section 5.2, we presented two alternative formulations for optimization subject to accessibility constraints, one with global formulation in (70) (based on total inaccessible volume), and one with local formulation in (73) (based on inaccessibility measure as a convolution field).

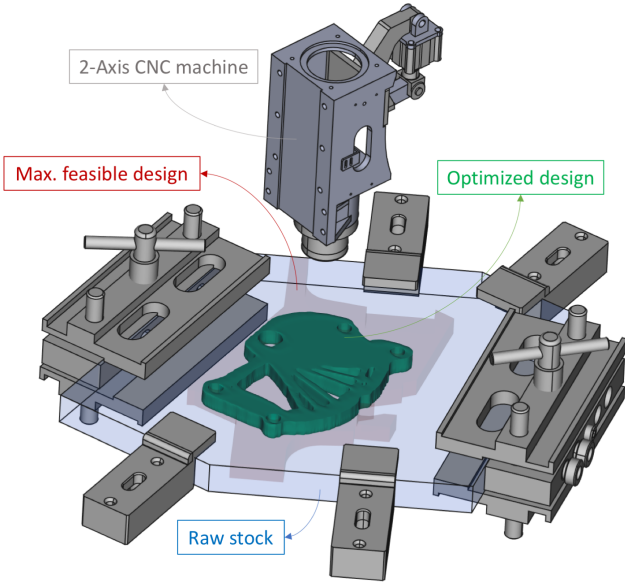


Figure 19: Optimized design at 40% volume fraction shown in the manufacturing setup.

Experimenting with the former fails, as expected, because the TSF for the global form is discontinuous, as elaborated in Section 5.8. The convolution field, on the other hand, is relatively well-behaved and can be used to penalize the TSF, as confirmed by our numerical experiments.

**Step 0.** In the absence of uncoupled pointwise constraints, start with the initial design domain  $\Omega_0 \in \mathcal{D}$ .

**Step 1.** The objective functions and constraints are given in (73). The additional constraint  $[\mathbf{1}_\Omega * \bar{\mathbf{1}}_T] = [0]$  requires that every point in the (voxelized) design  $[\mathbf{1}_\Omega]$  be accessible by the (voxelized) tool assembly  $[\mathbf{1}_T]$ , inverted as  $[\bar{\mathbf{1}}_T]$ . Remember that the convolution’s value at a given query point measures the volume of collision when the tool is displaced in such a way that a representative point on the tool – i.e., the origin of its local coordinate system in which  $[\mathbf{1}_T]$  is represented – is brought to the query point in the design domain.<sup>10</sup> We pick the origin of the tool at the tip of the cutter to simplify the formulation.

For the interior points, the constraint is obviously violated, because the tool cannot reach the interior without colliding with the part. The violation is larger for points that are farther from the boundary, providing a continuous penalty for TSF. Importantly, not every point in the exterior is accessible either. Even if the tip of the cutter does not collide with the part, the rest of the tool assembly might. The penalty is typically smaller for external

<sup>10</sup>Technically, the convolution field is defined over the configuration space of relative motions (translations in this case). The proper selection of the local coordinate system is important to “register” the convolution field with the design domain and other fields defined over it (e.g., TSF). See [65] for more details on the choice of origin.

points, as illustrated by Figs. 20 and 24. when there are more than one tool or approach orientations, the algorithm picks the minimum collision measure for penalization.

**Step 2.** The TSF for compliance is computed as usual, and is normalized by its maximum. An independent subroutine computes the convolution via FFTs, as discussed earlier, and is normalized by the volume of the tool (upper-bound to convolution). The TSF is penalized via convolution using an adaptive weight (for instance we start with  $\lambda_3 := 0.01$  and increase it to  $\lambda_3 := 0.2$  for lower volume fractions). Other design constraints such as minimum feature size or surface retainment can also be imposed as discussed in Section 2.

**Steps 3, 4.** The outer-loop iteration is as before. The inner loop iteration now cycles through one more FP-solver (the FFT-based convolution routine), as illustrated earlier in Fig. 13 (c).

Let us first consider a simple 2D cantilever beam of Fig. 20, with simple boundary conditions of a downward force  $\mathbf{F} = 1$  N, Young’s modulus of  $Y = 1$  GPa, and Poisson’s ratio of  $\nu = 0.3$ . Given a T-shaped tool with cutting part at the thin end, we consider accessibility in two scenarios with the tool approaching from one orientation (from left) and two orientations (from left and right). Figure 20 illustrates how the convolution fields differ in the two cases. Subsequently, the compliance TSF is penalized to capture accessibility under tool orientations.

Fig. 21 shows optimized shapes with and without the accessibility constraints with one and two tool orientations. Since the tool can only move in the plane, the TO cannot introduce interior holes without incurring a large penalty. Moreover, it can only remove material from the boundary in such a way that the remaining shape is machinable—e.g., no concave features of smaller feature size than the tool thickness in this case. Note that this is automatically enforced by penalizing convolution, without appealing explicitly to any notion of features or feature size.

In the case of the tool approaching at  $0^\circ$ , material can be accessed and removed only from the left side. However, with  $0^\circ$  and  $180^\circ$  angles for tool orientation, the material can be removed from both sides. Figure 22 shows the Pareto fronts of the three scenarios. As expected, optimization without accessibility constraint yields the best performance in terms of compliance while imposing accessibility with one approach direction significantly increases the compliance. However, when the tool can approach from both directions comparable performance to the unconstrained solutions can be achieved.

Let us next consider the car hood latch example of Fig. 15 one more time (also in 2D). Figure 23 shows the optimized latches at 35% volume fraction with and without the accessibility constraint. The same T-shaped tool is considered and oriented at both  $0^\circ$  and  $180^\circ$ . Imposing the accessibility constraint increased the relative compliance from 1.09 to 1.26. Figure 24 illustrates the original

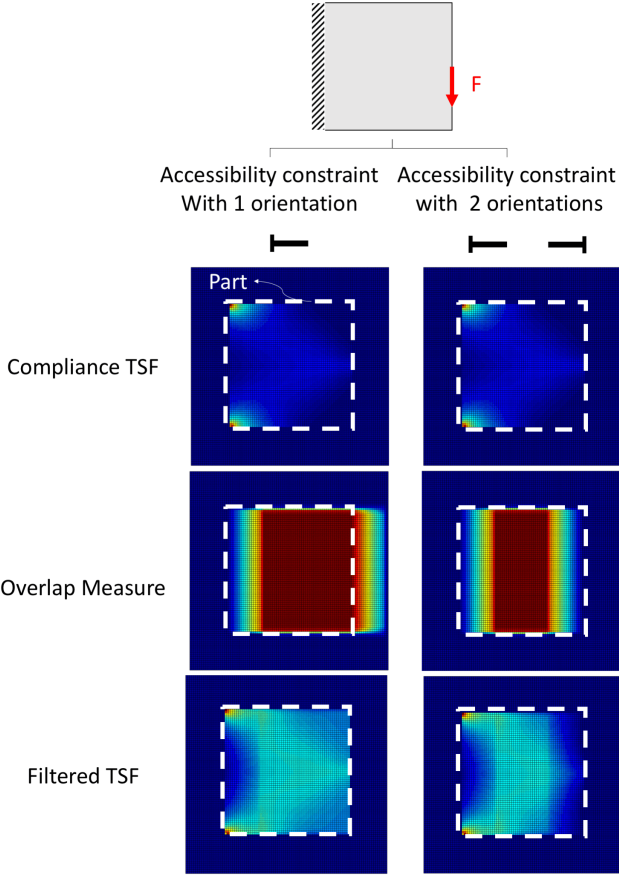


Figure 20: Penalizing TSF by the inaccessibility measure for T-shaped tool approaching from left (a) or from both left and right (b). Note that the field is asymmetric for the former.

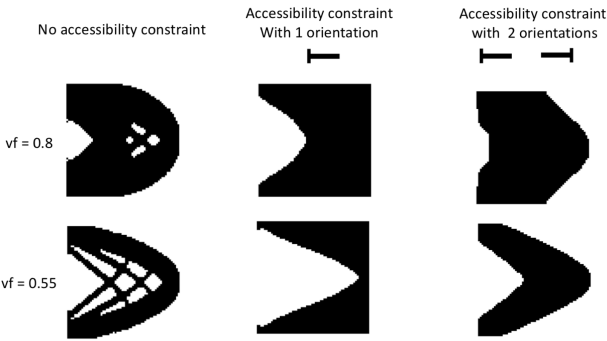


Figure 21: Optimized topologies at volume fractions 0.55 and 0.80 without accessibility constraint (a), with accessibility constraint for tool at  $0^\circ$  (b), and for tool at  $0^\circ$  and  $180^\circ$  (c).

TSF for compliance, the inaccessibility measure, and the penalized TSF for the hood latch at a volume fraction of 35%.

It should be noted that in the above examples, we only considered the collision between the tool and the part (i.e., no fixtures). Moreover, constraining the convolution field captures only the existence of final collision-free configura-

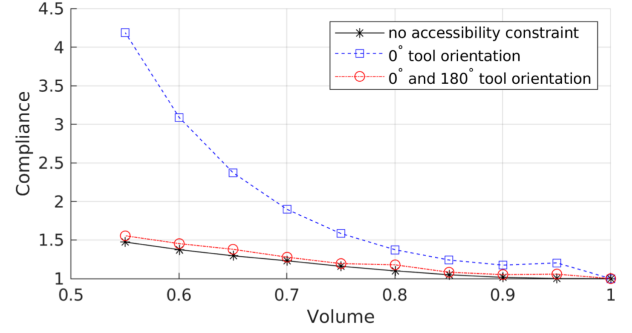


Figure 22: Pareto fronts of cantilever beam optimization without accessibility constraint, accessibility with tool only at  $0^\circ$  angle, and accessibility with tool at  $0^\circ$  and  $180^\circ$ .

tions for the tool to machine the part at different points in the design domain. It does not guarantee a collision-free tool-path from the initial tool configuration to the removal site. Path planning is beyond the scope of this paper.

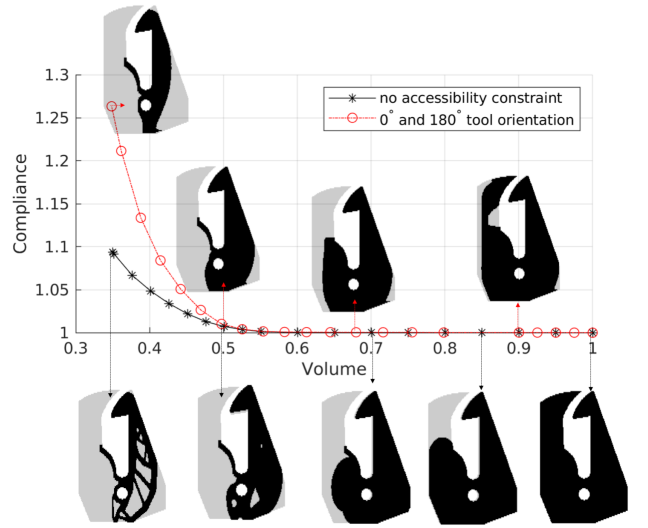


Figure 23: Pareto fronts of optimized designs for the hood latch, starting from the maximal pointset pruned via Unsweep, with and without accessibility constraint for tool at  $0^\circ$  and  $180^\circ$ .

### 5.8. Limitations of Sensitivity-Based Exploration

For the definition of the TSF in Section 5.3.1 to be valid, the limit in (75) must exist everywhere in the design domain and for all intermediate designs. In other words, puncturing the design with infinitesimal cavities must lead to infinitesimal changes in the violation of objective functions and constraints. For this to hold, the functions must be sufficiently smooth.<sup>11</sup> This is not always the case for general constraints.

<sup>11</sup>Technically, we need the function  $F_i : D_P^* \rightarrow \mathbb{R}$  to be differentiable in the Hausdorff topology of  $D_P^* = \mathcal{P}^*(\Omega_P^*)$ , which is relative to the topology of  $D = \mathcal{P}^*(\Omega_0)$ .



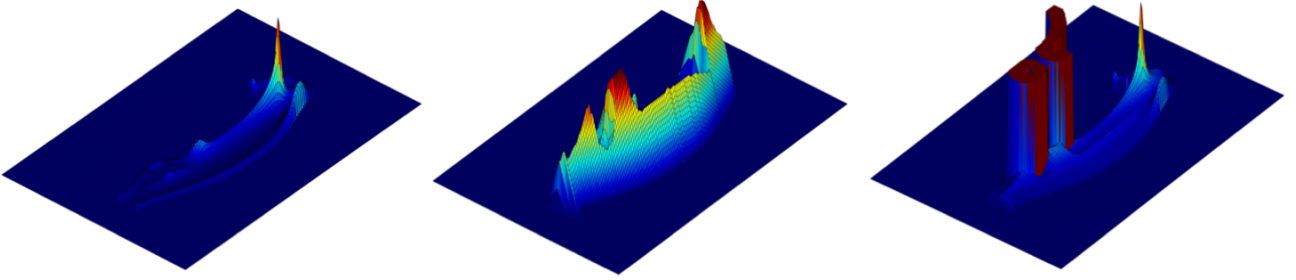


Figure 24: The original TSF for compliance (a), the inaccessibility measure obtained from a convolution of the design and tool at  $0^\circ$  and  $180^\circ$  (b), and the penalized TSF to incorporate accessibility and retain functional surfaces (c) for the final design at a volume fraction of 35%.

For example, if  $F_i(\Omega)$  is itself evaluating a topological property, introducing a puncture (no matter how small) can produce a large change in  $F_i(\Omega)$ . For example, topological defects in AM due to resolution limits can be characterized as integer-valued Euler characteristics [11, 12]. The Euler characteristic will increase by  $+1$  after adding a cavity, hence  $\mathcal{T}_i(\mathbf{x}; \Omega) \sim +1/O(\epsilon^3) \rightarrow +\infty$  as  $\epsilon \rightarrow 0^+$ . In practice, this appears as a discontinuity in constraint evaluation which adversely affects the convergence of the optimization loop (e.g., fixed-point iteration for PareTO).

As another example, recall the manufacturability constraint of (7) in which the total volume of inaccessible regions (for machining) was upper-bounded as a global constraint. Puncturing a hole of volume  $\text{vol}[B_\epsilon(\mathbf{x})]$  in the interior of the design adds exactly  $\text{vol}[B_\epsilon(\mathbf{x})]$  to the inaccessible volume, hence  $\mathcal{T}_i(\mathbf{x}; \Omega) = 1$  for all  $\mathbf{x} \in i\Omega$ . Most of the time, chipping off a visible (but too small)  $\text{vol}[\Omega \cap B_\epsilon(\mathbf{x})]$  adds the same exact amount to the inaccessible volume, because the tool is of finite size and cannot remove that volume in practice. However, it is possible that a substantial region of design that was initially inaccessible becomes accessible due to the small change at the boundary. Hence either  $\mathcal{T}_i(\mathbf{x}; \Omega) = 1$  or  $\mathcal{T}_i(\mathbf{x}; \Omega) \rightarrow -\infty$  for all  $\mathbf{x} \in \partial\Omega$ . This is not a well-behaved TSF for optimization.

The TSF is well-behaved for most global constraints that are defined as volumetric integrals of continuous physical fields (e.g., strain energy).<sup>12</sup> Small changes in the design often lead to small changes in physical response, when it is integrated over the entire domain, because integration smooths out the effects of local singularities. For instance, if we impose a constraint on the maximal stress as in (6), we cannot define a realistic TSF due to stress concentration. The simplest model of stress concentration yields an infinite maximal stress  $\sigma_\Omega(\mathbf{x}) \sim O(\epsilon^{-0.5})$  near an infinitesimal radius of curvature  $\epsilon \rightarrow 0^+$ , hence  $\mathcal{T}_i(\mathbf{x}; \Omega) \sim O(\epsilon^{-3.5}) \rightarrow +\infty$  when defined for the maximal stress as in (6). In practice, one can alleviate this issue by using a volumetric integral (e.g., the  $p$ -norm) of

stress rather than its maximum, in order to smooth out the effects of local singularities.

The other limitation with the usability of TSF is that the constraint function should not be locally “flat”. If the change in the violation of a constraint is too small, i.e., decays faster than  $O(\epsilon^3)$ , the limit will vanish and the TSF will not help the optimization. For example, manufacturability constraints that have to do with surface properties are insensitive to volumetric changes in design. We do not consider such cases in this paper.

In summary, the TSF formulation works well for global constraints that change smoothly with local volumetric material removal. Although this is not true for all global constraints, the good news is that some of them can be reformulated as local constraints. Therefore, we can use penalization of the local constraint (Section 5.3.3) instead of defining a TSF for the global constraint. For example, although the accessibility constraint that we discussed above does not yield a well-behaved TSF when treated as a global constraint  $g_3(\Omega) \leq 0$  of (7), we demonstrated in Section 5.7 that it can be successfully incorporated to constraint PareTO using penalization of the local form  $g_4(\mathbf{x}; \Omega) \leq 0$  of (14) in terms of inaccessibility measure defined as the convolution in (15).

## 6. Conclusions

Mechanical design requires simultaneous reasoning about multidisciplinary functional requirements and evaluating their trade-offs. These requirements are often expressed via heterogeneous types of constraints, including kinematics-based constraints for assembly and packaging, physics-based constraints for performance under mechanical or thermal loads, and both for manufacturability. Automated design optimization algorithms rarely consider all such requirements, and do not provide mechanisms to explore their trade space. For example, topology optimization can automatically generate designs with optimized material layouts for performance criteria such as strength and stiffness, but often ignores complex motion-based constraints imposed by collision avoidance in assembly or accessibility in manufacturing.

<sup>12</sup>This is the actual motivation behind using a volumetric measure of the inclusion in the denominator of (75) to normalize volumetric measures in the numerator. In principle, one can use a different measure for global constraints that vary at a different rate than  $O(\epsilon^3)$ .

### 6.1. Design Subspaces as First-Class Entities

The challenge in design space pruning and exploration is that IP-solvers are usually equipped with the tools to satisfy only a subset of the criteria in a multi-functional design problem. When these solvers are composed sequentially or in parallel, they can rarely provide guarantees to retain the other criteria satisfied by the preceding or concurrent solvers in the workflow. Moreover, most of the existing solvers generate a narrow subset of the design space—most commonly one or few design(s) that is/are deemed (locally or globally) “optimal” within the design subspace that appears feasible to the solver. Such *premature optimization* dramatically limits the subsequent solvers’ freedom to explore (best-case scenario) and might even get deadlocked at infeasible designs (worst-case scenario).

To solve such challenges, we follow a philosophy of treating *design spaces* (as opposed to individual *designs*) as *first-class entities*—at least to the extent that it is possible to do so by proper ordering of solvers in the workflow. This means that the entity being passed through the design pipeline—as input/output of consecutive synthesis solvers—is a design subspace described in its entirety by a representative object. This treatment allows postponing restrictive decisions and pushing premature optimization downstream as much as possible. We organize the design workflows by a careful analysis of the types of constraints and available solvers to address them and provide a systematic approach to compose FP- and IP-solvers depending on the type of design constraint(s) they can satisfy.

### 6.2. Pointwise Constraints & Maximal Designs

An important contribution of this work is a classification of constraints (namely, global, local, or strictly local) based on which the solvers are organized systematically in the computational design workflow. In particular, the strictly local (i.e., pointwise) constraints can be evaluated without a knowledge of the global shape, hence lead to a point membership classification (PMC) for a maximal design that satisfies them. The maximal pointset represents the entire feasible design subspace for a pointwise constraint, in the sense that containment in the maximal pointset is a necessary and sufficient condition for feasibility. As such, the design space can be pruned upfront by intersecting maximal pointsets of pointwise constraints, without premature optimization.

### 6.3. Other Constraints & Sensitivity Analysis

Most design criteria that depend on physics-based performance do not lead to a pointwise condition/PMC because the physical response of a design at any given point is typically dependent on the overall shape, i.e., the membership of one point is couple with the membership of other points. The dependency may be long-range, as in the case of static equilibrium throughout a mechanical structure, or local, as in transient dynamic effects within a bounded neighborhood over a finite time interval. In either case,

further design space pruning by means of PMC, to postpone decision making on the particular design layout, is not an option. In such cases, the FP-solvers collaborate in generating feasible and optimized designs by combining their sensitivity fields and methods such as fixed-point iteration for tracing the trade space of multiple objectives.

### 6.4. Duality of Forward & Inverse Problem Solvers

An important revelation of the classification is that the two different types of problems (namely, design space ‘pruning’ and ‘exploration’) demonstrate a different form of duality between forward and inverse problem (IP/FP)-solvers for *generative design*:

- For pointwise constraints, an IP-solver can be constructed from an FP-solver by generating a large sample of points in the design domain, applying the FP-solver in a pointwise fashion, evaluating the constraint, and retaining/discarding the ones that do/do not satisfy the constraint. In other words, the FP-solver provides a PMC test for the IP-solver. The process can be perfectly parallelized.
- For other constraints, an IP-solver can be constructed from an FP-solver by generating a number of candidate designs, evaluating the constraints, obtaining a sensitivity field to order the different points in the design according to their expected impact on the (dis)satisfaction of the constraint, removing the least sensitive points, and try again with the modified design. In other words, the FP-solver provides an evaluator for candidate designs to put in a feedback loop for the generate-and-test IP-solver. The process is a sequential loop that is repeated until convergence.

### 6.5. Limitations & Future Work

An important limitation of the approach is that it does not provide any guarantees for satisfying constraints that are neither pointwise nor differentiable, as exemplified in Section 5.8. For some local constraints (e.g., accessibility measures for machining), we have shown that penalizing the sensitivity fields of other global constraints with the local constraint can be effective. However, it is unclear how to systematically make such decisions with every new problem and constraint, unlike the case with pointwise constraints that are pruned upfront, or differentiable non-pointwise constraints that are filtered via local sensitivity analysis.

## Acknowledgments

This research was developed with funding from the Defense Advanced Research Projects Agency (DARPA). The views, opinions and/or findings expressed are those of the authors and should not be interpreted as representing the official views or policies of the Department of Defense or U.S. Government.

## References

- [1] O. Sigmund, K. Maute, Topology optimization approaches, *Structural and Multidisciplinary Optimization* 48 (6) (2013) 1031–1055.
- [2] N. P. van Dijk, K. Maute, M. Langelaar, F. van Keulen, Level-set methods for structural topology optimization: A review, *Structural and Multidisciplinary Optimization* 48 (3) (2013) 437–472.
- [3] G. I. N. Rozvany, A critical review of established methods of structural topology optimization, *Structural and Multidisciplinary Optimization* 37 (3) (2009) 217–237.
- [4] J. C. Latombe, *Robot Motion Planning*, Vol. 124, Springer Science & Business Media, 2012.
- [5] T. Lozano-Perez, Spatial planning: A configuration space approach, *IEEE Transactions on Computers* C-32 (2) (1983) 108–120. doi:10.1109/TC.1983.1676196.
- [6] S. Nelaturi, M. Lysenko, V. Shapiro, Rapid mapping and exploration of configuration space, *Journal of Computing and Information Science in Engineering* 12 (2) (2012) 021007.
- [7] S. Nelaturi, G. Burton, C. Fritz, T. Kurtoglu, Automatic spatial planning for machining operations, in: *Proceedings of the 2015 IEEE International Conference on Automation Science and Engineering (CASE'2015)*, 2015, pp. 677–682. doi:10.1109/CoASE.2015.7294158.
- [8] M. Behandish, S. Nelaturi, M. Allard, Automated process planning for turning: A feature-free approach, in: *Advances in Manufacturing Technology XXXII, Advances in Transdisciplinary Engineering Series, Volume 8*, 2018, pp. 45–50, proceedings of the International Conference on Manufacturing Research (ICMR'2018).
- [9] S. Nelaturi, W. Kim, T. Kurtoglu, Manufacturability feedback and model correction for additive manufacturing, *Journal of Manufacturing Science and Engineering* 137 (2) (2015) 021015. doi:10.1115/1.4029374.
- [10] S. Nelaturi, V. Shapiro, Representation and analysis of additively manufactured parts, *Computer-Aided Design* 67 (2015) 13–23.
- [11] M. Behandish, S. Nelaturi, Characterizing topological discrepancies in additive manufacturing, in: *Proceedings of the 28th Annual Fall Workshop on Computational Geometry (FWCG'2018)*, Association of Computing Machinery (ACM), 2018, pp. 71–74.
- [12] M. Behandish, A. M. Mirzendehtdel, S. Nelaturi, Detection and correction of topological errors in additive manufacturing, 2019, special Issue on the 23rd ACM Symposium on Solid and Physical Modeling (SPM'2019).
- [13] M. Behandish, S. Nelaturi, J. de Kleer, Automated process planning for hybrid manufacturing, Vol. 102, 2018, pp. 11–22, special Issue on the 22nd ACM Symposium on Solid and Physical Modeling (SPM'2018).
- [14] H. T. Ilies, V. Shapiro, On shaping with motion, *Journal of Mechanical Design* 122 (4) (2000) 567–574.
- [15] W. M. Lai, D. Rubinlor, E. Krempl, *Introduction to Continuum Mechanics*, 4th Edition, Butterworth-Heinemann Elsevier, 2009.
- [16] S. Nelaturi, M. Behandish, A. M. Mirzendehtdel, Automatic support removal for additive manufacturing post processing, 2019, special Issue on the 23rd ACM Symposium on Solid and Physical Modeling (SPM'2019).
- [17] J. G. Michopoulos, A. P. Iliopoulos, J. C. Steuben, A. J. Birnbaum, S. G. Lambrakos, On the multiphysics modeling challenges for metal additive manufacturing processes, *Additive Manufacturing* 22 (2018) 784–799.
- [18] A. M. Mirzendehtdel, K. Suresh, Support structure constrained topology optimization for additive manufacturing, *Computer-Aided Design* 81 (2016) 1–13.
- [19] H. T. Ilies, V. Shapiro, The dual of sweep, *Computer-Aided Design* 31 (3) (1999) 185–201. doi:10.1016/S0010-4485(99)00015-9.
- [20] K. Suresh, Efficient generation of large-scale Pareto-optimal topologies, *Structural and Multidisciplinary Optimization* 47 (1) (2013) 49–61.
- [21] M. L. Scott, *Programming Language Pragmatics*, Morgan Kaufmann, 2000.
- [22] J. Nocedal, S. J. Wright, *Numerical Optimization*, 2nd Edition, Springer, 2006.
- [23] M. R. Garey, D. S. Johnson, *Computers and Intractability*, Vol. 29, WH Freeman New York, 2002.
- [24] T. C. Koopmans, An analysis of production as an efficient combination of activities, *Activity Analysis of Production and Allocation*.
- [25] A. Charnes, W. W. Cooper, B. Golany, L. Seiford, J. Stutz, Foundations of data envelopment analysis for Pareto-Koopmans efficient empirical production functions, *Journal of econometrics* 30 (1-2) (1985) 91–107.
- [26] O. B. Augusto, F. Bennis, S. Caro, Multiobjective engineering design optimization problems: A sensitivity analysis approach, *Pesquisa Operacional* 32 (3) (2012) 575–596.
- [27] S. Sra, S. Nowozin, S. J. Wright, *Optimization for Machine Learning*, Mit Press, 2012.
- [28] S. Lienhard, C. Lau, P. Müller, P. Wonka, M. Pauly, Design transformations for rule-based procedural modeling, in: *Computer Graphics Forum*, Vol. 36, Wiley Online Library, 2017, pp. 39–48.
- [29] E. K. Burke, G. Kendall, J. Newall, E. Hart, P. Ross, S. Schulenburg, Hyper-heuristics: An emerging direction in modern search technology, in: *Handbook of metaheuristics*, Springer, 2003, pp. 457–474.
- [30] E. K. Burke, M. Gendreau, M. Hyde, G. Kendall, G. Ochoa, E. Özcan, R. Qu, Hyper-heuristics: A survey of the state of the art, *Journal of the Operational Research Society* 64 (12) (2013) 1695–1724.
- [31] P. A. Vikhar, Evolutionary algorithms: A critical review and its future prospects, in: *The 2016 International Conference on Global Trends in Signal Processing, Information Computing and Communication (ICGTSPICC)*, IEEE, 2016, pp. 261–265.
- [32] Z. Michalewicz, Genetic algorithms, numerical optimization, and constraints, in: *Proceedings of the 6th International Conference on Genetic Algorithms*, Vol. 195, Citeseer, 1995, pp. 151–158.
- [33] J. Kennedy, *Swarm intelligence*, in: *Handbook of Nature-Inspired and Innovative Computing*, Springer, 2006, pp. 187–219.
- [34] Y. Shi, Particle swarm optimization, *IEEE Connections* 2 (1) (2004) 8–13.
- [35] R. Storn, K. Price, Differential evolution—a simple and efficient heuristic for global optimization over continuous spaces, *Journal of Global Optimization* 11 (4) (1997) 341–359.
- [36] H. A. Eschenauer, N. Olhoff, Topology optimization of continuum structures: A review, *Applied Mechanics Reviews* 54 (4) (2001) 331.
- [37] J. D. Deaton, R. V. Grandhi, A survey of structural and multidisciplinary continuum topology optimization: Post 2000, *Structural and Multidisciplinary Optimization* 49 (1) (2013) 1–38.
- [38] L. Wang, P. K. Basu, J. P. Leiva, Automobile body reinforcement by finite element optimization, *Finite Elements in Analysis and Design* 40 (8) (2004) 879–893.
- [39] E. Kessler, W. J. Vankan, Multidisciplinary design analysis and multi-objective optimisation applied to aircraft wing (2006).
- [40] J. J. Alonso, P. LeGresley, V. Pereyra, Aircraft design optimization, *Mathematics and Computers in Simulation* 79 (6) (2009) 1948–1958.
- [41] V. Coverstone-Carroll, J. W. Hartmann, W. J. Mason, Optimal multi-objective low-thrust spacecraft trajectories, *Computer Methods in Applied Mechanics and Engineering* 186 (2-4) (2000) 387–402.
- [42] L. Harzheim, G. Graf, A review of optimization of cast parts using topology optimization, *Structural and Multidisciplinary Optimization* 31 (5) (2005) 388–399.
- [43] O. Sigmund, On the design of compliant mechanisms using

- topology optimization, *Journal of Structural Mechanics* 25 (4) (1997) 493–524.
- [44] M. P. Bendsøe, O. Sigmund, Material interpolation schemes in topology optimization, *Archive of Applied Mechanics* 69 (9-10) (1999) 635–654.
- [45] O. Sigmund, Design of multiphysics actuators using topology optimization-part II: Two-material structures, *Computer Methods in Applied Mechanics and Engineering* 190 (49-50) (2001) 6605–6627.
- [46] M. P. Bendsøe, O. Sigmund, *Topology Optimization*, Springer Berlin Heidelberg, Berlin, Heidelberg, 2004.
- [47] G. Allaire, F. Jouve, A. M. Toader, A level-set method for shape optimization, *Comptes Rendus Mathématique* 334 (12) (2002) 1125–1130.
- [48] G. Allaire, F. De Gournay, F. Jouve, A. Toader, Structural optimization using topological and shape sensitivity via a level set method, *Control and Cybernetics* 34 (1) (2005) 59.
- [49] D. N. Chu, Y. M. Xie, A. Hira, G. P. Steven, Evolutionary structural optimization for problems with stiffness constraints, *Finite Elements in Analysis and Design* 21 (4) (1996) 239–251.
- [50] X. Huang, Y. M. Xie, Bi-directional evolutionary topology optimization of continuum structures with one or multiple materials, *Computational Mechanics* 43 (3) (2008) 393–401.
- [51] X. Liu, W. J. Yi, Q. S. Li, P. S. Shen, Genetic evolutionary structural optimization, *Journal of Constructional Steel Research* 64 (3) (2008) 305–311.
- [52] M. K. Thompson, G. Moroni, T. Vaneker, G. Fadel, R. I. Campbell, I. Gibson, A. Bernard, J. Schulz, P. Graf, B. Ahuja, F. Martinaj, Design for additive manufacturing: Trends, opportunities, considerations, and constraints, *CIRP Annals* 65 (2) (2016) 737–760.
- [53] I. Pandelidis, Q. Zou, Optimization of injection molding design. part I: Gate location optimization, *Polymer Engineering & Science* 30 (15) (1990) 873–882.
- [54] B. H. Lee, B. H. Kim, Optimization of part wall thicknesses to reduce warpage of injection-molded parts based on the modified complex method, *Polymer-Plastics Technology and Engineering* 34 (5) (1995) 793–811.
- [55] J. Petersson, O. Sigmund, Slope constrained topology optimization, *International Journal for Numerical Methods in Engineering* 41 (8) (1998) 1417–1434.
- [56] P. M. Pandey, K. Thrimurthulu, N. V. Reddy, Optimal part deposition orientation in FDM by using a multicriteria genetic algorithm, *International Journal of Production Research* 42 (19) (2004) 4069–4089.
- [57] A. S. Nezhad, F. Barazandeh, A. R. Rahimi, M. Vatani, Pareto-based optimization of part orientation in stereolithography, *Proceedings of the Institution of Mechanical Engineers, Part B: Journal of Engineering Manufacture* 224 (10) (2010) 1591–1598.
- [58] R. Paul, S. Anand, Optimization of layered manufacturing process for reducing form errors with minimal support structures, *Journal of Manufacturing Systems* 36 (2015) 231–243.
- [59] A. T. Gaynor, J. K. Guest, Topology optimization considering overhang constraints: Eliminating sacrificial support material in additive manufacturing through design, *Structural and Multidisciplinary Optimization* 54 (5) (2016) 1157–1172.
- [60] M. Langelaar, Topology optimization of 3D self-supporting structures for additive manufacturing, *Additive Manufacturing* 12 (2016) 60–70.
- [61] X. Qian, Undercut and overhang angle control in topology optimization: A density gradient based integral approach, *International Journal for Numerical Methods in Engineering* 111 (3) (2017) 247–272.
- [62] A. M. Mirzendehdel, K. Suresh, *A Hands-On Introduction to Topology Optimization*, CreateSpace Independent Publishing Platform, 2017.
- [63] C. Schmutzler, F. Bayerlein, S. Janson, C. Seidel, M. F. Zaeh, Pre-compensation of warpage for additive manufacturing, in: *Fraunhofer Direct Digital Manufacturing Conference (DDMC)*, 2016, pp. 392–399.
- [64] A. M. Mirzendehdel, B. Rankouhi, K. Suresh, Strength-based topology optimization for anisotropic parts, *Additive Manufacturing* 19 (2018) 104–113.
- [65] M. Lysenko, S. Nelaturi, V. Shapiro, Group morphology with convolution algebras, in: *Proceedings of the 14th ACM Symposium on Solid and Physical Modeling (SMP’2010)*, ACM, 2010, pp. 11–22.
- [66] M. Behandish, H. T. Ilies, Analytic methods for geometric modeling via spherical decomposition, *Computer-Aided Design* 70 (2015) 100–115, special Issue on the 19th ACM Symposium on Solid and Physical Modeling (SPM’2015).
- [67] K. D. Wise, A. Bowyer, A survey of global configuration-space mapping techniques for a single robot in a static environment, *The International Journal of Robotics Research* 19 (8) (2000) 762–779.
- [68] P. Y. Papalambros, The optimization paradigm in engineering design: Promises and challenges, *Computer-Aided Design* 34 (12) (2002) 939–951.
- [69] N. D. Mankame, G. K. Ananthasuresh, Topology optimization for synthesis of contact-aided compliant mechanisms using regularized contact modeling, *Computers & structures* 82 (15-16) (2004) 1267–1290.
- [70] P. Kumar, A. Saxena, R. A. Sauer, Computational synthesis of large deformation compliant mechanisms undergoing self and mutual contact, *Journal of Mechanical Design* 141 (1) (2019) 012302.
- [71] M. Luo, Y. and Li, Z. Kang, Topology optimization of hyperelastic structures with frictionless contact supports, *International Journal of Solids and Structures* 81 (2016) 373–382.
- [72] K. Suresh, A 199-line Matlab code for Pareto-optimal tracing in topology optimization, *Structural and Multidisciplinary Optimization* 42 (5) (2010) 665–679.
- [73] A. A. G. Requicha, Representations for rigid solids: Theory, methods, and systems, *ACM Computing Surveys (CSUR)* 12 (4) (1980) 437–464.
- [74] L. E. Kavvaki, Computation of configuration-space obstacles using the fast Fourier transform, *IEEE Transactions on Robotics and Automation* 11 (3) (1995) 408–413. doi:10.1109/70.388783.
- [75] R. B. Tilove, A. A. G. Requicha, Closure of Boolean operations on geometric entities, *Computer-Aided Design* 12 (5) (1980) 219–220.
- [76] J. Serra, *Image Analysis and Mathematical Morphology*, Academic Press, Inc., 1983.
- [77] S. Nelaturi, V. Shapiro, Configuration products and quotients in geometric modeling, *Computer-Aided Design* 43 (7) (2011) 781–794.
- [78] A. A. Novotny, R. A. Feijoo, E. Taroco, C. Padra, Topological sensitivity analysis for three-dimensional linear elasticity problem, *Computer Methods in Applied Mechanics and Engineering* 196 (41) (2007) 4354–4364.
- [79] R. L. Burden, J. D. Faires, *Numerical analysis*, Brooks, Cole, Belmont, CA.
- [80] K. Suresh, M. M., Stress-constrained topology optimization: A topological level-set approach, *Structural and Multidisciplinary Optimization* 48 (2) (2013) 295–309.
- [81] A. M. Mirzendehdel, K. Suresh, A Pareto-optimal approach to multimaterial topology optimization, *Journal of Mechanical Design* 137 (10).
- [82] S. Deng, K. Suresh, Multi-constrained topology optimization via the topological sensitivity, *Structural and Multidisciplinary Optimization* 51 (5) (2015) 987–1001.
- [83] S. Deng, K. Suresh, Multi-constrained 3d topology optimization via augmented topological level-set, *Computers & Structures* 170 (2016) 1–12.